Two-proton-transfer reactions ^{208}Pb(^{12}C, ^{10}Be)^{210}Po and ^{208}Pb(^{16}O, ^{14}C)^{210}Po†

F. D. Becchetti,* D. G. Kovar,‡ B. G. Harvey, D. L. Hendrie, H. Homeyer,§ J. Mahoney, W. von Oertzen,‖ and N. K. Glendenning

Lawrence Berkeley Laboratory, University of California, Berkeley, California 94720

(Received 4 September 1973)

Levels in ^{210}Po have been investigated using the two-proton-transfer reactions (^{12}C, ^{10}Be) and (^{16}O, ^{14}C) on ^{208}Pb at incident energies $E(^{12}C) = 78$ MeV and $E(^{16}O) = 104$ and 140 MeV. Reaction products were identified and energies measured with a magnetic spectrometer and a focal-plane resistive-wire proportional counter. Many levels in ^{210}Po were observed up to an excitation energy of about 8 MeV. The results have been analyzed using distorted-wave Born approximation, and shell-model wave functions for levels in ^{210}Po have been tested. The $0^+ \rightarrow 0^+$(g.s.) transition is enhanced by a factor ~8 compared with the expected strength for a pure $(\pi h_{9/2})^2$ 0^+ configuration for ^{210}Po(g.s.). The dependence of the cross sections on projectile and target structure is discussed.

[NUCLEAR REACTIONS ^{208}Pb(^{12}C, ^{10}Be), $E = 78$ MeV; ^{208}Pb(^{16}O, ^{14}C), $E = 104$, 140 MeV; measured $\sigma(E_f, \theta)$; DWBA analysis; ^{210}Po levels deduced structure; ^{209}Bi(^{12}C, ^{11}B), $E = 78$ MeV; ^{209}Bi(^{16}O, ^{15}N), $E = 104$ MeV; measured $\sigma(E_f)$, ^{210}Po levels deduced relative spectroscopic factors; Resolution 100–200 keV.]

I. INTRODUCTION

Many shell-model calculations have been performed predicting levels in nuclei consisting of a few particles or holes outside of a ^{208}Pb core. Most of these nuclei can be studied with a variety of light-ion reactions. To date, however, the levels in ^{210}Po formed by transferring two protons directly to the ^{208}Pb core have not been studied. In this paper we report the observation of levels in ^{210}Po via the heavy-ion two-proton-transfer reactions: (^{12}C, ^{10}Be) and (^{16}O, ^{14}C). The results are used to test predictions of available shell-model wave functions.

II. EXPERIMENTAL PROCEDURE

The experiments were performed using ^{12}C (E_L = 78 MeV) and ^{16}O (E_L = 104, 140 MeV) beams from the Lawrence Berkeley Laboratory (LBL) 88-in. cyclotron. The beam was energy dispersed across the target by a pair of analyzing magnets.[1] Reaction products were detected in the focal plane of a dispersion-matched magnetic spectrometer with a position-sensitive proportional counter (six horizontal wires, 6×45-cm^2 effective area) backed by a plastic scintillator.[2] A schematic diagram of the apparatus is shown in Fig. 1. The focal-plane counter is described in detail elsewhere.[2,3] The counter system measures $B\rho$ (position), energy loss ($\Delta E/\Delta X$), time-of-flight (TOF), and a scintillator output (energy) for heavy-ion-reaction products. This information is sufficient to give unambiguous particle identification. In the present arrangement a time-zero detector[4] consisting of a thin (~80-μg/cm^2) NE111 plastic scintillator was placed at the entrance of the spectrometer (see Fig. 1). The signal from this detector and another from the final scintillator were used for the TOF measurement (replacing the cyclotron rf signal employed previously[2]). Typical resolutions [full width at half maximum (FWHM)] in the present experiment were $\Delta E/\Delta X \sim 10\%$, TOF ~1% (2.5 nsec), and energy resolution $\delta E/E$ ~0.15% or approximately 100–150 keV for (^{12}C, ^{10}Be) and 120–200 keV for (^{16}O, ^{14}C), depending on the target thickness. (The TOF resolution is limited by the differences in particle flight paths through the spectrometer.) Charge and mass separation up to $A \sim 20$ was obtained. A two-dimensional spectrum of $\Delta E/\Delta X$ vs TOF is shown in Fig. 2. Energy spectra for different particle groups are obtained by setting gates on $\Delta E/\Delta X$ and TOF.[2,3]

Both "thin" (~100-μg/cm^2) and "thick" (~300-μg/cm^2) targets consisting of ^{208}Pb evaporated onto thin carbon foils (10–30 μg/cm^2) were used. Some of the targets also had a layer of carbon evaporated over the ^{208}Pb so as to reduce evaporation and sputtering of the ^{208}Pb from beam bombardment. In order to reduce the latter effects we limited the beam currents to $\lesssim$300 nA (fully stripped ions).

Cross sections were obtained from the particle yields relative to a monitor counter and the ^{16}O (8^+) yield, which in turn, was normalized to Rutherford cross sections at forward angles. The targets were oriented such that reaction products exited through a thickness of carbon sufficient

to ensure charge equilibrium. Measurements of yields to various charge states indicated that the reaction products were predominantly (≥80%) fully stripped. Therefore cross sections were calculated from the measured yields of the fully stripped ions, corrected by an appropriate factor.[3]

The energy calibration of the focal-plane counter was obtained by sweeping elastically scattered particles across the detector by varying the spectrometer field in known steps. The results were parametrized in such a way that the energy of any particle could be determined from its position measurement to an accuracy ~±0.05% (±30 to ±70 keV). The data used to obtain the energy calibration were also used to generate parameters which allowed position spectra from the six individual wires to be added together to form a single spectrum.

Several spectra were obtained using thin targets (~100 $\mu g/cm^2$) to accurately determine the position and relative intensity of levels. Thick targets (~300 $\mu g/cm^2$) were then used to obtain angular distributions.

III. EXPERIMENTAL RESULTS

A. Spectra

Particle spectra obtained for the reactions ^{208}Pb-(^{12}C, ^{10}Be)^{210}Po, $E(^{12}C) = 78$ MeV and ^{208}Pb(^{16}O, ^{14}C)-^{210}Po, $E(^{16}O) = 104$ MeV are shown in Figs. 3 and 4.

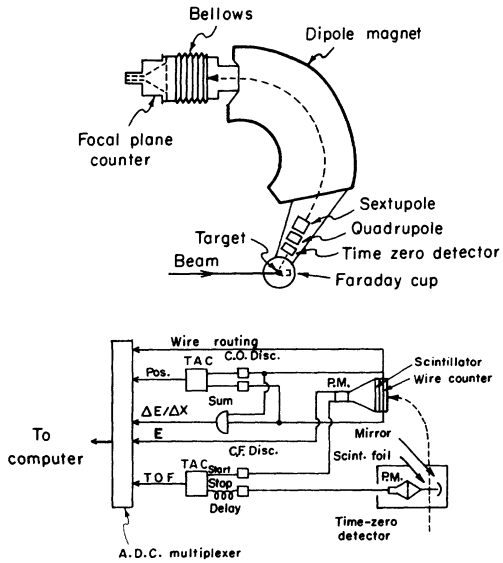

FIG. 1. Schematic diagram of experimental apparatus. Top: Spectrometer. Bottom: Electronics for focal-plane counter. The dashed curves represent particle trajectories.

The ^{12}C and ^{16}O bombarding energies correspond to the same projectile velocities and nearly the same energy above the Coulomb barrier (~20 MeV greater). In Fig. 4 the angle (52.2° lab) is near the peak in the measured angular distributions, which are similar for the two reactions to all levels (see Sec. III B). Several ^{14}C spectra for ^{208}Pb(^{16}O, ^{14}C)^{210}Po at $E(^{16}O) = 140$ MeV were also obtained. Although the energy resolution is poorer at the higher bombarding energy, one observes that most of the states seen at $E(^{16}O) = 104$ MeV are populated.

The shapes of the spectra shown in Figs. 3 and 4 reflect the strong Q-value dependence of heavy-ion reactions.[5,6] This dependence results in a "Q window" whose centroid Q_{opt} depends on the charge-transfer and bombarding energy.[5] Semiclassical theory[5] predicts for sub-Coulomb reactions $Q_{opt} \approx E_1(Z_t/Z_1)$ where E_1 is the incident c.m. energy, Z_t is the charge transferred to the projectile, and Z_1 is the projectile charge (assumed here to be much smaller than the target charge). This gives $Q_{opt} \approx -25$, -24, and -33 MeV or $E_x = 6.6$, 10.4, and 19.4 MeV for ^{208}Pb(^{12}C, ^{10}Be), $E_L = 78$ MeV and ^{208}Pb(^{16}O, ^{14}C), $E_L = 104$ and 140 MeV,

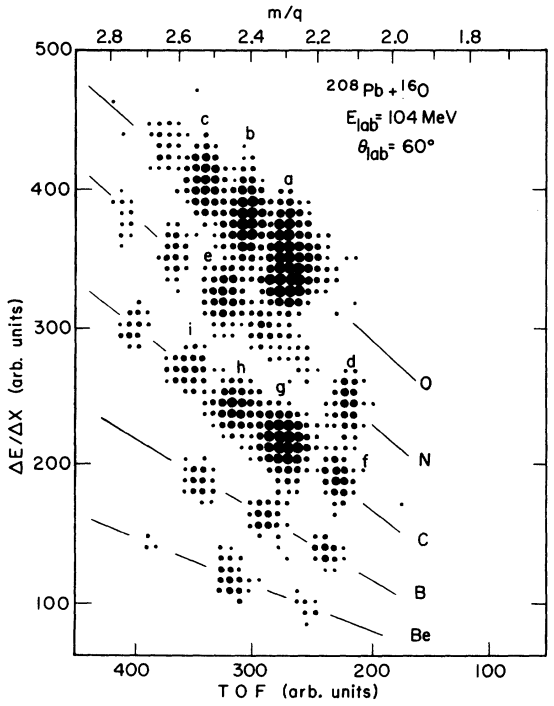

FIG. 2. An energy loss ($\Delta E/\Delta X$) vs time-of-flight (TOF) spectrum at the spectrometer field setting (Fig. 3) for ^{14}C (6^+). $\Delta E/\Delta X$ and TOF have been corrected for dependence on $B\rho$ (Ref. 2). m/q (top) is the approximate mass to charge ratio for the groups indicated: a: ^{18}O (7^+); b. ^{17}O (7^+); c: ^{18}O (7^+); d: ^{15}N (7^+); e: ^{15}N (6^+); f: ^{13}C (6^+); g: ^{14}C (6^+); h: ^{12}C (5^+); i: ^{13}C (5^+).

respectively. No-recoil distorted-wave Born-approximation (DWBA) calculations ($L \sim 0$), however, give $Q_{opt} \approx -14$ MeV for all of these reactions while calculations with recoil give $Q_{opt} \approx -18$ MeV. (See Appendix.) The data appear to indicate $E_x \approx 4$, 7.5, and 15 MeV, respectively, i.e., the observed Q_{opt} values are slightly more positive than those given by the semiclassical approximation and more negative than those given by DWBA. The exact shapes of the spectra, however, are complicated functions of both the Q dependence of the reaction and the structure of the final states.

The particle groups observed in the present experiment and their partial integrated cross sections are presented in Table I. The groups listed can in principle consist of both ^{210}Po and the outgoing products (^{14}C and ^{10}Be) being in particle-stable excited states. ^{10}Be has such known[7] levels $E_x(J^\pi) = 3.37(2^+)$, $5.96(1^-, 2^+)$, $6.18(0^+)$, and $6.26(2^-)$ MeV while for ^{14}C (Ref. 8): $E_x(J^\pi) = 6.09(1^-)$, $6.59(0^+)$, $6.73(3^-)$, $6.90(0^-)$, $7.01(2^+)$, and $7.34(2^-)$ MeV. Groups from outgoing particles in excited states have been observed in (^{16}O, ^{15}N) and (^{12}C, ^{11}B) at $E_L = 104$ and 78 MeV on Zr and Mo targets and are observed to be substantially (200–700 keV) broadened, apparently by γ decay in flight.[3] A comparison of the position and widths of levels observed in the different reactions indicated that groups seen with $E_x < 5.5$ MeV are due to levels in ^{210}Po, with the exception of a group seen in (^{12}C, ^{10}Be) at $E_x = 3.41$ MeV which could be ^{10}Be* (3.37 MeV). The weak intensity seen would be consistent with the results of a ^{18}O-(^{12}C, ^{10}Be)^{20}Ne experiment[9] in which this level was not populated. There are indications, however, that some groups with $E_x > 6$ MeV observed in (^{16}O, ^{14}C) are due to excitation of ^{14}C (see Figs. 3 and 4), particularly the groups at $E_x \sim 7$ MeV.

B. Angular distributions

Angular distributions are shown in Figs. 5 and 6. A few forward-angle points for some of the levels observed in (^{16}O, ^{14}C) were obscured by contaminants. The error bars shown reflect only the statistical errors (standard deviations) in the estimated total yield and background correction. The fluctuations in the data at $E_x > 6$ MeV may not be significant owing to the level density and background at high excitation.

The shapes of the angular distributions for $E_x < 6$ MeV are essentially the same to within the errors indicated even though known states of very different spins ($J^\pi = 0^+$ to 8^+) are shown (see Sec. IV). This lack of "J signature" has been noted previously for (^{16}O, ^{15}N) etc. on heavy target nuclei[10] and greatly limits the usefulness of heavy-ion reactions in extracting spins for these nuclei. As observed in a comparison of the ^{208}Pb(^{12}C, ^{11}B)-^{209}Bi and ^{208}Pb(^{16}O, ^{15}N)^{209}Bi reactions[10] it may be possible to obtain spectroscopic information from the comparison of heavy-ion reactions involving different projectiles. As seen in Fig. 4 there are some notable differences in the spectra shown, e.g., the population of the levels at $E_x = 3.7$ and 4.0 MeV. We discuss this further in Sec. V E.

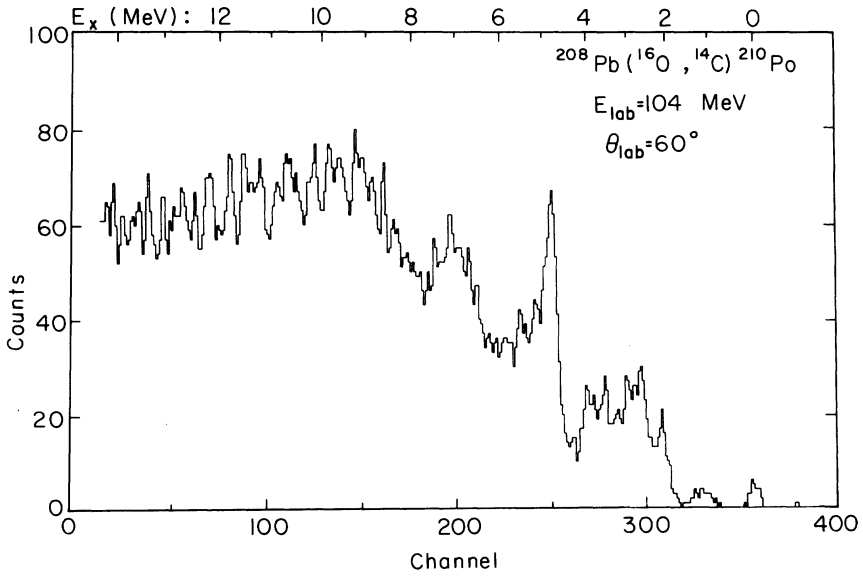

FIG. 3. A position spectrum (summed over six wires) for ^{14}C (6^+) (thick target), $E_L = 104$ MeV. Excitation energies are given in Table I.

IV. KNOWN LEVELS IN ^{210}Po

The low-lying levels in ^{210}Po have been studied previously by several means: (i) the decay of ^{210}At (Ref. 11); (ii) the ^{208}Pb(α, $2n$-γ) reaction[12, 13]; (iii) inelastic scattering[14] and proton pickup[15] from ^{210}Po; and (iv) the (α, t) and (^{3}He, d) reactions[16, 17] on ^{209}Bi.

Of these studies (iv) is of most interest here since ^{209}Bi(α, t) and ^{209}Bi(^{3}He, d) should populate states of the form $[\pi lj \otimes \pi h_{9/2}]_J$ outside of a ^{208}Pb core. It is also possible to reach such states via the heavy-ion reactions (^{12}C, ^{11}B) and (^{16}O, ^{15}N). In Fig. 7 we compare the results[16, 17] of ^{209}Bi(α, t)-^{210}Po and ^{209}Bi(^{3}He, d)^{210}Po with spectra from (^{12}C, ^{11}B) and (^{16}O, ^{15}N). It can be seen that the heavy-ion reactions populate the same levels as

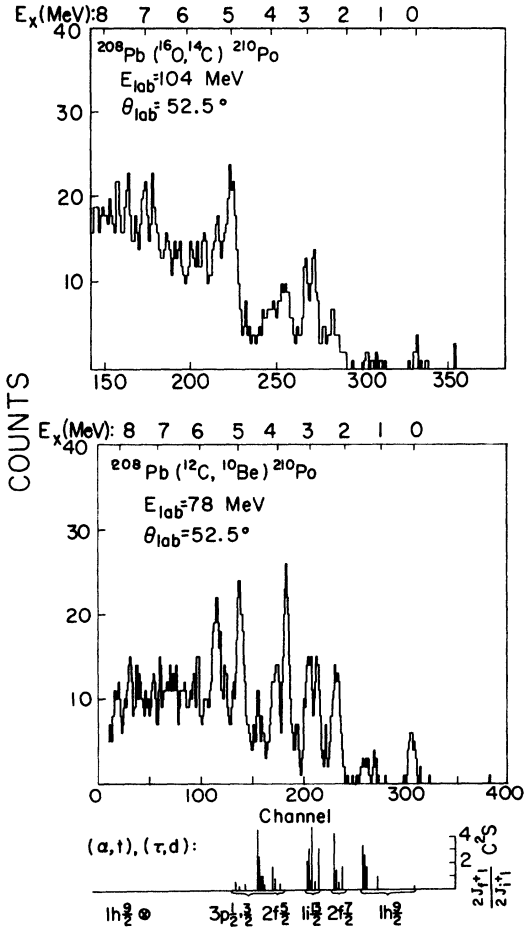

FIG. 4. Top: A comparison of (^{16}O, ^{14}C) and (^{12}C, ^{10}Be) spectra (thin target) near the grazing angle. The energy scales have been adjusted to be approximately the same. Bottom: Excitation energies and spectroscopic factors for ^{210}Po levels $[1h_{9/2} \otimes nlj]_J$ observed in ^{209}Bi(α, t) and ^{209}Bi(^{3}He, d), Refs. 16 and 17.

in (α, t) and (^{3}He, d) (although adjacent members of a multiplet are not always resolved). In Table II we list the levels in ^{210}Po believed[16, 17] to be $[\pi lj \otimes \pi h_{9/2}]$ and compare calculated spectroscopic factors relative to those of single-particle states in ^{209}Bi observed[10] in ^{208}Pb(^{12}C, ^{11}B) and ^{208}Pb-(^{16}O, ^{15}N) at the same bombarding energies. The results are consistent with the light-ion results[16, 17] and we therefore conclude that the heavy-ion reactions proceed via a direct single-step transfer without appreciable core excitation. As in the reaction[10] ^{208}Pb→ ^{209}Bi we observe a j selectivity which depends on the structure of the projectile. The (^{16}O, ^{15}N) reaction ($nlj = 1p_{1/2}$) favors final states involving transitions with the single-particle orbits $j = l + \frac{1}{2}$ compared to (^{12}C, ^{11}B) ($nlj = 1p_{3/2}$). Furthermore, single-particle wave functions with large radial extension (large n) are favored.

The known levels in ^{210}Po and some of their properties are given in Table III. The levels observed in ^{209}Bi(α, t)^{210}Po and ^{209}Bi(^{3}He, d) are also indicated in Figs. 4 and 7.

V. DWBA CALCULATIONS

A. Cross section

Since kinematic effects play a dominant role in heavy-ion reactions, it is necessary to account for these before attempting to deduce spectroscopic information. Fortunately DWBA theory appears to reproduce kinematic effects reasonably well,[6] although some details remain questionable.[10, 18, 19]

The cross section for the transfer of two identical nucleons from spinless projectiles $A(a, b)B$, where $a = b + 2$ and $B = b + 2$, can be written in the "no-recoil" approximation (see Appendix) as[20-22]

$$\frac{d\sigma}{d\Omega} = \frac{2J_B + 1}{2J_A + 1} \frac{d\sigma^{\mathrm{DW}}}{d\Omega}(\theta). \tag{1}$$

J_A and J_B are the initial and final target spins, respectively. In the special cases considered here ($J_a = J_b = 0$, $\Delta T = 1$, and $\Delta S = 0$) we have $J_A = 0$ (π_i = positive) so that $L = J = J_B$ and $\pi_f = (-1)^L$, i.e., only transitions to states of natural parity are allowed.

B. Form factors

Various methods have recently been devised to calculate the form factors for heavy-ion two-nucleon transfers.[23-27] The problem is substantially more complicated than for light-ion reactions such as (t, p) etc. since a zero-range interaction would not be appropriate for projectiles such as ^{16}O and ^{12}C. In addition, the transferred nucleons occupy single-particle states other than $1s_{1/2}$ as

in light ions such as t and α and therefore the relative motion of these nucleons may be more complex.

We have used two methods to calculate form factors. Both methods are applicable for the simultaneous transfer of two nucleons (in contrast to a sequential transfer). One method computes the form factor as a matrix element of the sum of the shell-model interactions that bind the transferred nucleons to the projectile core. We refer to this as the "sum of interactions" (SI). The other method approximates the sum of the interactions by a single potential acting on the center of mass of the transferred nucleons. We refer to this as the "center-of-mass interaction" (CMI). Both the CMI and SI methods yield a local form factor which depends only on the separation R between projectile and target core, and the angular momentum transfer. Thus Eq. (1) can be calculated with conventional "no-recoil" DWBA programs. Corrections to DWBA due to recoil can also be included, as described in the Appendix.

A detailed comparison of the SI and CMI methods as applied to two-proton transfers may be found

TABLE I. Groups observed in this experiment.

^{208}Pb(^{12}C, ^{10}Be)^{210}Po E_L = 78 MeV		^{208}Pb(^{16}O, ^{14}C)^{210}Po E_L = 104 MeV		^{208}Pb(^{16}O, ^{14}C)^{210}Po E_L = 140 MeV	
E_x [a] (MeV)	$\int\sigma$ [b] (μb)	E_x [c] (MeV)	$\int\sigma$ [d] (μb)	E_x [e] (MeV)	σ (37.5°) (μb/sr)
0	94 ± 15	0	47 ± 15	0	16 ± 4
1.19	36 ± 9	1.14	23 ± 10	0.75	9 ± 3
1.46 [f]	46 ± 11 [f]	1.47	37 ± 14	1.42	31 ± 6
2.27 [f]	300 ± 30 [f]	2.32	205 ± 30	2.29	65 ± 7
2.56	55 ± 8	2.51	41 ± 13 [g]	...	...
2.85	214 ± 21	2.84	247 ± 31 [g]	3.01	108 ± 11
3.05 [f]	291 ± 29 [f]	3.08	182 ± 20 [g]	...	...
3.41 [f,h]	83 ± 19 [f,h]	...	...	...	...
3.70	394 ± 31	3.70	281 ± 32 [g]	3.74	104 ± 11
4.07 [f]	247 ± 24 [f]	4.06	217 ± 31 [g]	4.12	68 ± 7
4.36	41 ± 8	...	...	...	...
4.53	70 ± 11	4.50	91 ± 27	...	...
4.95	366 ± 29	...	...	...	...
5.07	122 ± 17	5.03 [f]	682 ± 79 [f]	4.95	128 ± 8
5.33 [f]	199 ± 23 [f]	...	...	5.27	60 ± 6
5.53 [h]	450 ± 36 [h]	5.43 [f]	289 ± 34 [f]	...	...
5.81	82 ± 15	5.68	189 ± 34	5.71	149 ± 15
6.06	173 ± 20	6.04	203 ± 25	...	...
6.29	66 ± 16	6.29	200 ± 25	...	...
6.49	60 ± 9	...	...	...	...
6.76 [f]	96 ± 15 [f]	6.71	250 ± 30	...	...
...	...	6.93 [h]	311 ± 34 [h]	6.84 [h]	159 ± 15 [h]
7.38	96 ± 17	7.25 [h]	357 ± 36 [h]	...	...
7.75 [f]	182 ± 26 [f]	7.66	336 ± 35	7.63	169 ± 16
8.1	...	...	...	...	...
...	...	8.71	384 ± 38	8.77	183 ± 18
...	...	9.44	393 ± 39	9.23	93 ± 14
...	...	9.95	265 ± 27	10.02	209 ± 20
...	...	10.26	256 ± 27	...	...
...	...	10.66	504 ± 50	10.81	386 ± 25
...	...	11.02	289 ± 29	...	...
...	...	11.40	386 ± 39	...	...
...	...	11.70	...	11.66	341 ± 25
...	...	12.30	...	12.17	291 ± 20

[a] ±30 keV, E_x < 6 MeV; ±50 keV, E_x > 6 MeV.
[b] Integrated cross section θ = 44 to 82° (c.m.). Statistical errors are given.
[c] ±40 keV, E_x < 6 MeV; ±60 keV, E_x > 6 MeV.
[d] Integrated cross section θ = 33 to 79° (c.m.) except as noted. Statistical errors are given.
[e] ±60 keV.
[f] Unresolved group of states.
[g] Integrated θ = 40 to 79° (c.m.).
[h] May be due to projectile excitation (see Sec. VII).

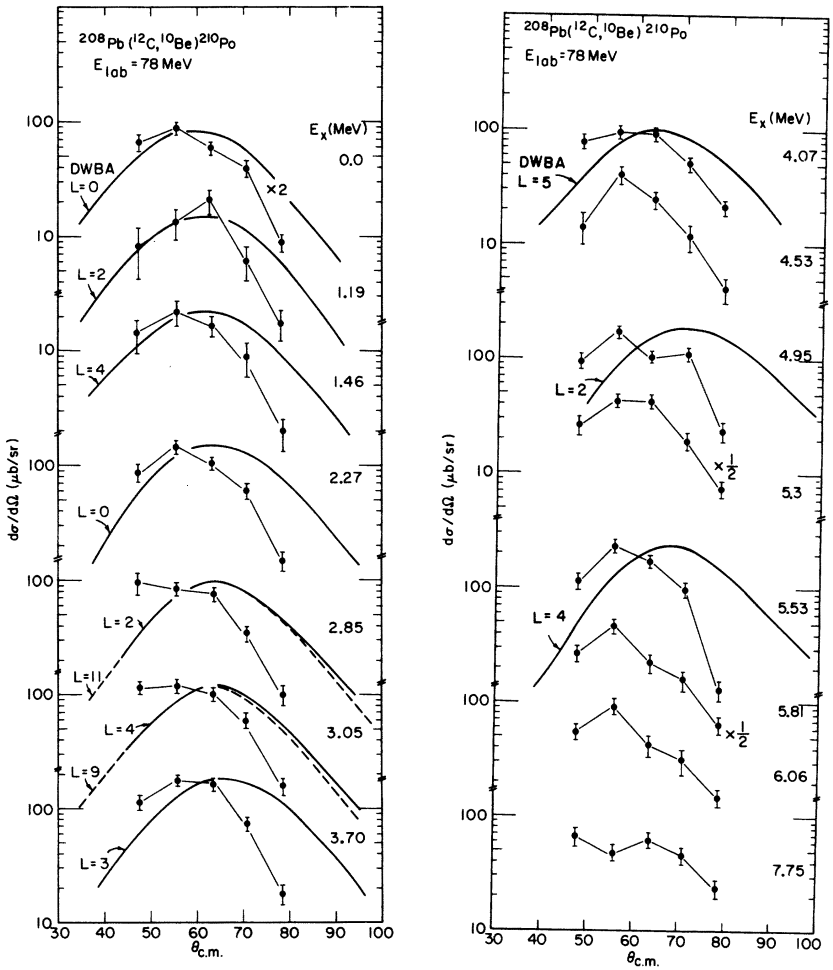

FIG. 5. Angular distributions for groups observed in ^{208}Pb(^{12}C, ^{10}Be). The smooth curves are no-recoil DWBA calculations (see Sec. V D). The data points have been connected to guide the eye.

TABLE II. Comparison of spectroscopic factors for ^{210}Po and ^{209}Bi.

Reaction	E_x [a] (MeV)	$d\sigma/d\Omega$ (mb/sr)	Assumed s.p. [c]	Ratio [b] $C^2S(^{210}\text{Po})/C^2S(^{209}\text{Bi})$
^{209}Bi(^{12}C, ^{11}B)^{210}Po	1.18	0.16 ± 0.04	$1h_{9/2}$	0.73 ± 0.08
E_L = 78 MeV	1.52	1.10 ± 0.11		
θ_L = 65°	2.37	1.92 ± 0.14	$2f_{7/2}$	0.70 ± 0.06
	2.94	0.44 ± 0.07	$1i_{13/2}$	0.89 ± 0.10
	3.20	0.65 ± 0.08		
	4–5.8	2.12 ± 0.21	$2f_{5/2}$-$3p$	1.03 ± 0.11
^{209}Bi(^{16}O, ^{15}N)^{210}Po	1.55	0.25 ± 0.02	$1h_{9/2}$	0.92 ± 0.09
E_L = 104 MeV	2.40	2.64 ± 0.08	$2f_{7/2}$	0.95 ± 0.04
θ_L = 67.5°	3.11	0.79 ± 0.04	$1i_{13/2}$	0.90 ± 0.04
	4–5.8	3.33 ± 0.13	$2f_{5/2}$-$3p$	1.14 ± 0.04

[a] Excitation energy of centroid (±50 keV). See Fig. 7.

[b] Ratio of summed spectroscopic factors for levels in ^{210}Po and ^{209}Bi as deduced from cross-section ratios using ^{209}Bi data from Ref. 10.

[c] States in ^{210}Po assumed to be multiplets formed by coupling single-particle configuration listed to ^{209}Bi ($1h_{9/2}$) g.s.

in the Appendix. Both methods give the same qualitative results although quantitative differences exist. These differences are greatest when the transfer proceeds by states having small relative SI motion [e.g., $0^+ \rightarrow (1h_{9/2})^2 0^+$]. Comparisons of various methods as applied to two-nucleon transfers may be found in Ref. 23.

C. Kinematic effects

The cross sections observed in heavy-ion reactions are determined in large part by kinematic effects. These effects arise from the high localization of the reactions in coordinate and angular momentum space. The net results are Q windows whose width and magnitude depend on the l transfer L. The reaction kinematics are discussed in more detail in the Appendix. The cross sections $E_x \leq 8$ MeV are predicted to increase with L $(=J)$ up to $L \approx 6$ and then drop for $L > 6$. The reaction (^{12}C, ^{10}Be), which has Q values $< Q_{\text{opt}}(L=0)$, should favor larger L transfers than (^{16}O, ^{14}C).

Spectroscopic considerations, of course, must also be included when comparing the two reactions (see Sec. V E). We find, however, that the kinematics and spectroscopy can often be separated in an approximate manner [see Eqs. (A1)–(A2)].

D. Angular distributions

We have calculated angular distributions for (^{12}C, ^{10}Be) and (^{16}O, ^{14}C) using the DWBA program DWUCK with form factors calculated with both CMI and SI methods, the former with a radial cutoff at 8.5 fm (see Appendix). Some of the calculations are shown in Figs. 5 and 6 (SI form factor). The calculated shapes of the angular distributions are nearly independent of L or the nuclear configurations. The maxima in the DWBA angular distributions shift back in angle with increasingly negative Q value whereas the experimental results do not. This is shown in Fig. 8 where we plot the calculated (CMI method) and observed peak angle in the cross sections. The

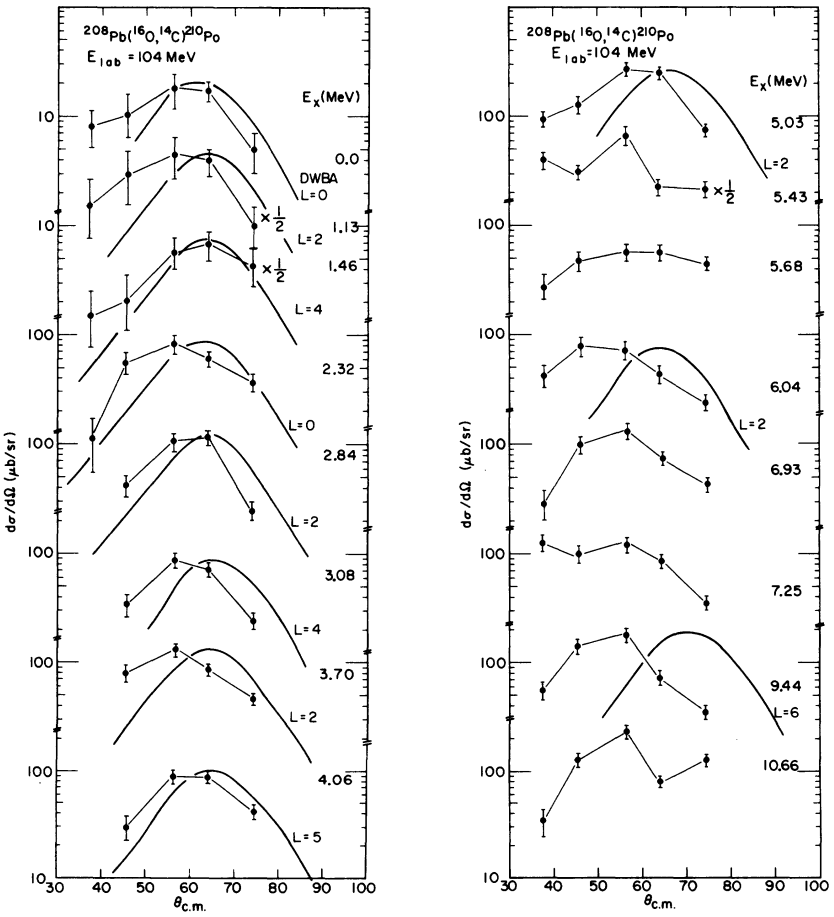

FIG. 6. Angular distributions for groups observed in ^{208}Pb(^{16}O, ^{14}C). The smooth curves are no-recoil DWBA calculations (see Sec. V D). The data points have been connected to guide the eye.

latter were determined by shifting the calculated curves by eye to fit the data. Results similar to those shown in Figs. 5, 6, and 8 have also been observed for single-nucleon transfers on ^{208}Pb (Refs. 10 and 28) and other mass regions.[29-31] The discrepancies between theory and experiment appear to be associated with the optical-model description of the distorted waves in DWBA, since the quality of the fits are correlated[29] with projectile orbit mismatch ($Q - Q_{opt}$) as can be noted in Figs. 5, 6, and 8 ($Q_{opt} \sim -14$ MeV).

The calculations can be brought into better agreement with experiment by adjusting optical-model parameters,[30] e.g. decreasing the half radius R by ~0.6 fm. The resulting parameters do not then yield fits to the elastic scattering of ^{16}O and ^{12}C from ^{208}Pb. We have therefore chosen, instead, to use optical parameters which fit the elastic scattering in the incident channels and compare the DWBA calculations with integrated or peak cross sections.

One of the effects not included in the DWBA calculations above is that due to recoil. Such effects are found to be important for certain types of single-nucleon transfers between heavy ions where L transfers are restricted by a parity rule arising from the no-recoil assumption. The L transfer for two-proton transfers with $J_a = J_b = J_A = 0$, however, are *a priori* restricted to $L = J_B$. Recoil, then, alters the DWBA amplitude in the manner suggested by Buttle and Goldfarb[32] and should be minimal when $Q \approx Q_{opt}$. We have estimated recoil effects by comparing "no-recoil" and "recoil" DWBA calculation for a dinucleon cluster transfer (Sec. I of Appendix). The shapes of the angular distributions are not significantly altered by the inclusion of recoil, i.e., the discrepancies vs Q value persist.

E. Sensitivity to nuclear structure

The single-proton transfers (^{12}C, ^{11}B) and (^{16}O, ^{14}C) are observed to be j dependent.[10] The former reaction proceeds by transfer of a $j_> \equiv l + \frac{1}{2}$ proton while the latter proceeds via transfer of a

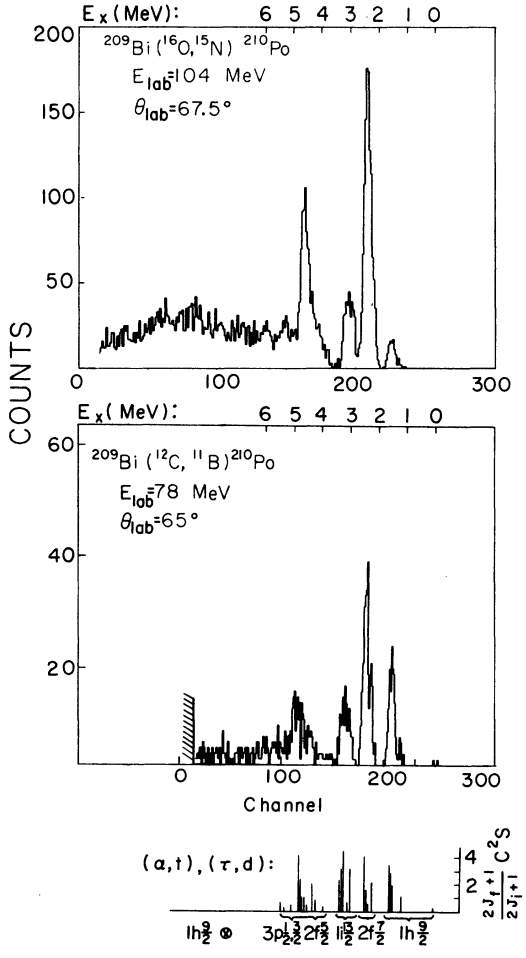

FIG. 7. Top: Spectra (near the grazing angle) for the single-proton transfers (^{16}O, ^{15}N) and (^{12}C, ^{11}B) on ^{209}Bi. Bottom: Position and spectroscopic factors for levels in ^{210}Po observed in ^{209}Bi(α, t) and ^{209}Bi$(^3$He$, d)$, Refs. 16 and 17.

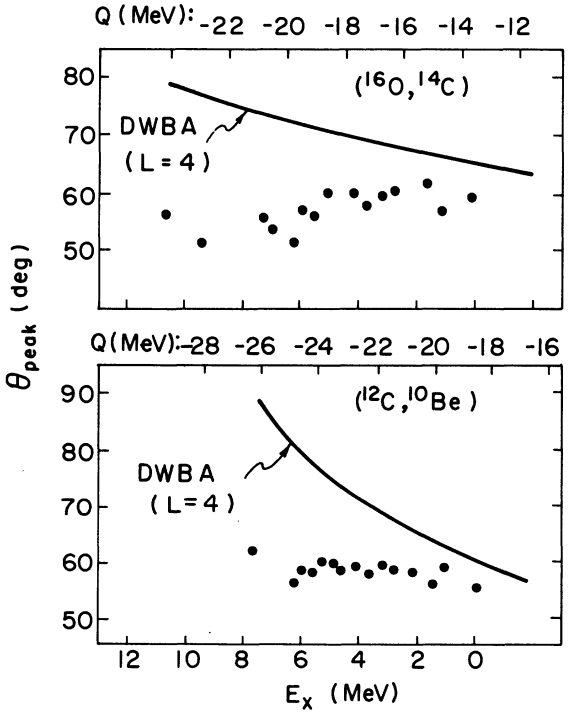

FIG. 8. Experimental (●) and calculated (V_{CMI} method) peak angle in $d\sigma/d\Omega$ for ^{208}Pb(^{16}O, ^{14}C), $E_L = 104$ MeV and ^{208}Pb(^{12}C, ^{10}Be), $E_L = 78$ MeV. The calculation shown is for $L = 4$ (see Figs. 5 and 6).

TABLE III. Levels in ^{210}Po.

Previous work				This work	
E_x [a] (MeV)	J^π [b]	G_λ [c] (s.p.u.)	$[J_f/J_i]C^2S$ [d]	E_x [e] (MeV)	J^π [f]
0	0^+		0.18	0	(0^+)
1.181	2^+	3.5 ± 1.5	1.05	1.19	(2^+)
1.437	4^+	(weak)	1.82		
1.473	6^+		2.65	1.46	$(4^+ + 6^+ + 8^+)$
1.556	8^+		3.30		
2.188	8^+		1.91		
...	...	...	...	2.27	$(0^+ + 8^+)$
2.290	$(2^+, 3^+)$	(weak)	0.47		
2.336	6^+		1.40		
2.382	4^+		(1.1)		
2.387	3^-	46 ± 15			
2.403	5^+		(1.3)		
2.405	(1^+)				
2.413	3^+		(0.7)		
2.438	7^+		(1.6)		
...	...	...	...	2.56	(2^+)
2.658 [c]		(weak)			
2.849	11^-		3.10		
...	...	...	...	2.85	(2^+)
2.874 [c]		(weak)			
2.910	5^-	13 ± 4	0.54		
2.999	(9^-)		(1.6)		
3.009	(2^-)				
3.017	7^-		(3.2)		
3.026	5^-	16 ± 5			
...	...	...	...	3.05	(4^+)
3.075	4^-		0.75		
3.111	(3^-)				
3.125	6^-		(1.2)		
3.138	(8^-)		(1.8)		
3.183	10^-		2.33		
3.428	(4^-)				
3.437 [c]		(weak)		3.41 [g]	
3.525	$(5, 6)^-$				
3.699	$(4^\pm, 5^\pm, 6^\pm)$				
...	...	...	...	3.70	(3^-)
3.711	$(4^\pm, 5^\pm, 6^\pm)$				
3.727	$(5)^-$				
3.780	$(4^-, 5^-, 6^-)$		~0.5		
3.801 [c]		(weak)			
4.032 [d]		(weak)	~1		
4.105 [c]		(weak)		4.07	(5^-)
4.142 [d]		(weak)	~2		
4.237 [c]		(weak)			
4.336 [d]			~0.5		
4.324 [h]	11^-				
4.346 [c]		(weak)			
4.372 [h]	13^-				
4.377 [d]		(weak)	~1	4.36	
4.466 [d]			~1		

TABLE III *(Continued)*

Previous work				This work	
E_x [a] (MeV)	J^π [b]	G_λ [c] (s.p.u.)	$[J_f/J_i]C^2S$ [d]	E_x [e] (MeV)	J^π [f]
4.542 [d]			~2.5	4.53	(6^+)
4.636 [d]			~4		
4.666 [d]					
4.777 [h]	13^-				
4.948 [d]			~0.5		
...	...	...	...	4.95	(2^+)
...	...	...	...	5.07	(4^+)
5.058 [h]	16^+				
5.151 [d]			weak		
5.223 [d]			~0.5		
...	...	...	...	5.33	
				5.53 [g]	
				5.81	
				6.06	
				6.29	
				6.49	
				6.76	
				6.93 [g]	
				7.38	
				7.75	
				(see Table I)	

[a] Excitation in ^{210}Po taken from compilation of data given in Ref. 11 except as noted. Errors typically $<\pm 3$ keV.

[b] Taken from compilation Ref. 11 except as noted.

[c] (p,p') results (Ref. 14). Errors in E_x ± 10 keV.

[d] References 16 and 17.

[e] Results from (^{12}C, ^{10}Be) except as noted. Errors ± 30 keV, $E_x < 6$ MeV ± 50 keV, $E_x > 6$ MeV (see also Table I and Fig. 9).

[f] The spins listed are suggested assignments based on shell-model predictions and calculated transition strengths (see Sec. VII and Fig. 9). The data, however, do not contain unambiguous spin signatures which permit direct spin assignments.

[g] May be due to projectile excitation (see Sec. VII).

[h] $(\alpha, 2n\gamma)$ results (Refs. 12 and 13).

$j_< \equiv l - \frac{1}{2}$ $(1p_{1/2})$ proton. The (^{16}O, ^{15}N) reaction is found to favor transitions to $j_>$ target states compared to (^{12}C, ^{11}B), i.e., the preferred transitions[5, 10] are $j_>$(projectile)$\rightarrow j_<$(target) and $j_<$(projectile)$\rightarrow j_>$(target).

Calculations for heavy-ion-induced two-proton transfers (see Appendix) indicate a similar j selectivity in that

$$(j_>)^2\text{(projectile)} \rightarrow (j_<)^2\text{(target)} \qquad (2a)$$

and

$$(j_<)^2\text{(projectile)} \rightarrow (j_>)^2\text{(target)} \qquad (2b)$$

are favored in the limits of pure jj coupling. Most of this j selectivity is destroyed by configuration mixing, however. Thus, calculations with "realistic," i.e., LS or intermediate-coupling projectile wave functions exhibit much less j dependence than would be expected with jj coupling. Nonetheless, significant differences in cross sections (~2) are expected for the (^{12}C, ^{10}Be) and (^{16}O, ^{14}C) reactions due to projectile structure alone.

Besides a dependence on the single-nucleon j values, the calculations for (^{12}C, ^{10}Be) and (^{16}O, ^{14}C) also indicate a dependence on J, the total spin of the target state. Two types of transitions can be classified:

$$\text{Type I: } 0^+\text{(projectile)} \rightarrow [j_< j'_<]_J \text{ or } [j_> j'_>]_J\text{(target)} \qquad (3a)$$

and

$$\text{Type II: } 0^+\text{(projectile)} \rightarrow [j_< j'_>]_J \text{ or } [j_> j'_<]_J\text{(target)}. \qquad (3b)$$

Type I transition strengths decrease with increasing J while Type II transition strengths in-

crease with J (see Appendix).

The j and J selectivity noted above together with the kinematic selectivity (Sec. V C) greatly limits the type of state which can be populated strongly in (^{12}C, ^{10}Be) or (^{16}O, ^{14}C). It is apparent from Fig. 4 that these reactions are selective. Out of ~50 possible two-proton states available below 8-MeV excitation energy only ~10 levels are strongly populated in each reaction.

VI. COMPARISON WITH EXPERIMENT: TEST OF SHELL-MODEL WAVE FUNCTIONS FOR ^{210}Po

A. Spectra and angular distributions

In Sec. V E above we considered pure shell-model configurations for ^{210}Po. Calculations[33-35] and experiments[11-17] indicate, however, that configuration mixing must be included. We have investigated two shell-model calculations for ^{210}Po: that of Kuo-Herling (KH) which uses matrix elements deduced from nucleon-nucleon scattering,[34] and that of Ma-True (MT) which uses matrix elements calculated from a phenomenological force[35] (central + multipolar). Both calculations reproduce many of the properties for nuclei A ~208: energy levels, spectroscopic factors, transition rates, etc. In Fig. 9 we compare schematically predictions for levels in ^{210}Po with previously reported levels[11-17] and groups seen in the present experiment. Figures 10 and 11 compare the experimental spectra for (^{12}C, ^{10}Be) and (^{16}O, ^{14}C) with calculations (SI method) using

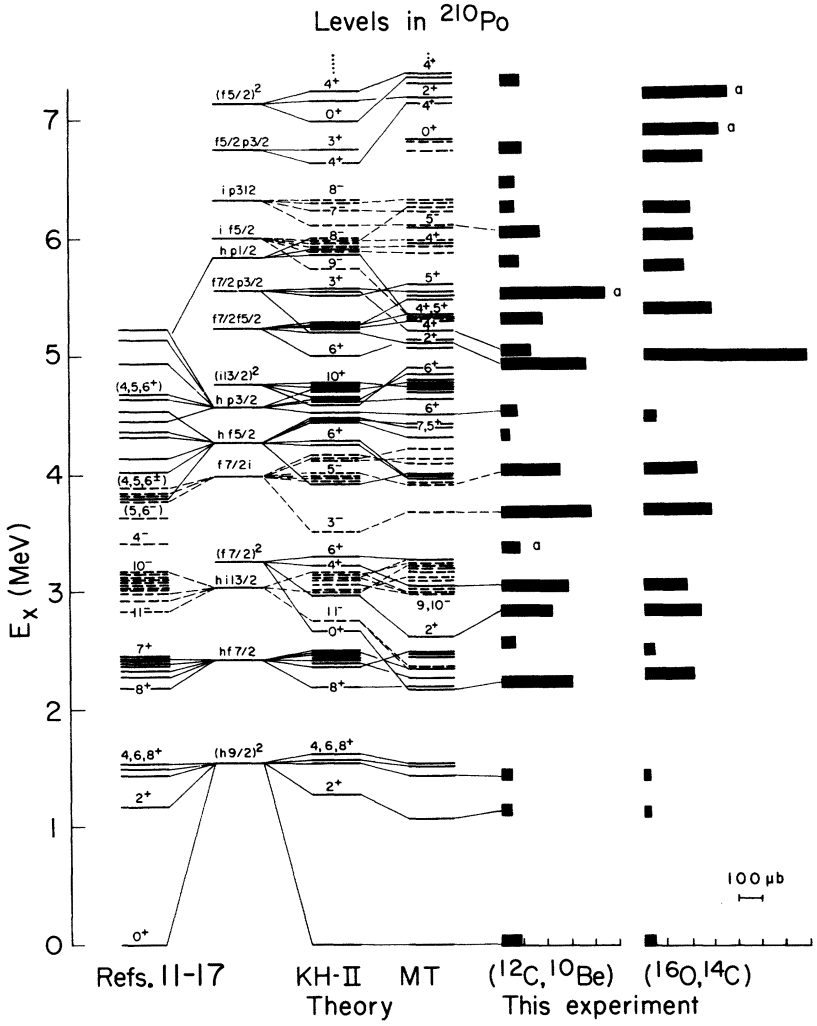

FIG. 9. A comparison of previously known (Refs. 11–17) and predicted (Refs. 34 and 35) levels in ^{210}Po with groups observed in this experiment. The bar graphs represent integrated cross sections (see Table I). Groups labeled "a" could be due to projectile excitation (see Sec. VII). Suggested level assignments (see text) are indicated by connecting lines: —— positive parity; --- negative parity.

Cohen-Kurath (CK) wave functions[36,37] for the projectiles and MT wave functions for ^{210}Po. We have included a correction for recoil effects in the calculations (see Appendix). The qualitative features of the spectra are reproduced, i.e., the number of levels and the distribution of transition strength, although the g.s. strength appears to be overestimated. Relatively few configurations dominate: $(f_{7/2}p_{3/2})$, $(f_{7/2}{}^2)$, $(f_{7/2}i_{13/2})$, $(f_{7/2}p_{1/2})$, $(f_{7/2}, f_{5/2})$, with the strengths spread via configuration mixing. There appears to be more than one candidate for each observed level $E_x > 2$ MeV, however, and unfortunately, the calculated angular distributions are nearly independent of J. This is shown in Figs. 5 and 6 where we compare DWBA calculations with experiment (SI method, CK, and MT wave functions). The DWBA curves shown have been normalized to the peak cross section. As noted in Sec. V D the calculated curves have approximately the correct (L-independent) shapes, but the peak positions shift with Q value (or E_x) much faster than the data indicate (see Fig. 8).

The lack of appreciable L signature makes it difficult to make specific level assignments which are not very model-dependent. The projectile and final-state selectivity noted by Eqs. (2) and (3) can be utilized to suggest the likely spin and configuration for a given level. In Sec. VII we will enumerate the likely candidates for the levels observed in (^{16}O, ^{14}C) and (^{12}C, ^{10}Be). These candidates are indicated in Fig. 9.

B. Ground-state band

1. *Relative intensities*

The 0^+ (g.s.), 2^+ (1.18-MeV), and 4^+, 6^+, 8^+ (1.44–1.56-MeV) levels in ^{210}Po are well isolated from other expected levels (see Fig. 9) and were observed in both (^{12}C, ^{10}Be) and (^{16}O, ^{14}C). The cross sections are given in Table I. The 4-8$^+$ multiplet was not resolved so we consider here the summed cross sections to the individual states.

In Table IV we compared relative cross sections

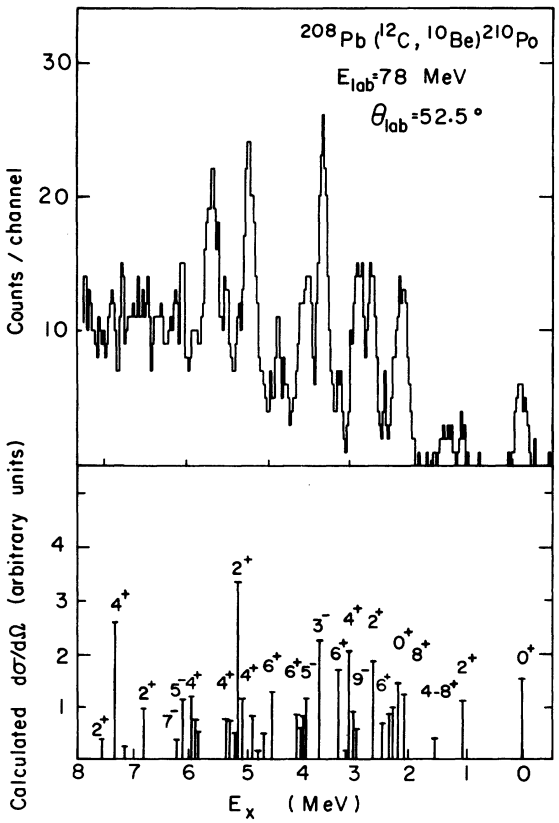

FIG. 10. Observed (top) and calculated (bottom) spectra for (^{12}C, ^{10}Be). The calculations (V_{SI} method) use CK (Refs. 36 and 37) and MT (Ref. 35) wave functions and have been arbitrarily normalized. Corrections for recoil have been included in the DWBA calculations (see text).

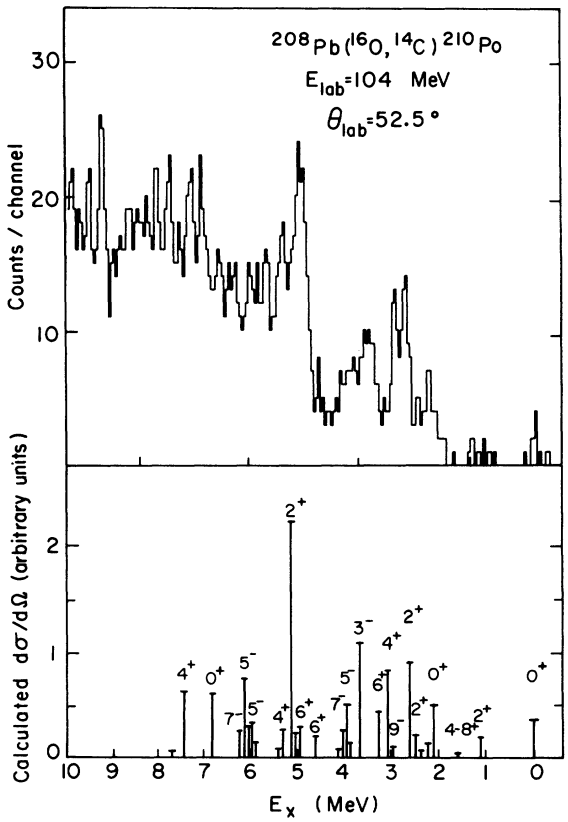

FIG. 11. Observed (top) and calculated (bottom) spectra for (^{16}O, ^{14}C). The calculations (V_{SI} method) use CK (Refs. 36 and 37) and MT (Ref. 35) wave functions and have been arbitrarily normalized. Corrections for recoil have been included in the DWBA calculations (see text).

for the 0^+, 2^+, and unresolved $4\text{-}8^+$ levels calculated assuming various wave functions: pure $(1h_{9/2})^2$, KH-I, and KH-II,[34] and MT.[35] Also included are calculations for ^{210}Po 0^+ g.s. using single-particle amplitudes deduced[15] from the proton-pickup reaction ^{210}Po(t, α) and assuming constructive phases between amplitudes. The form factor was calculated with the SI method and CK wave functions for ^{12}C and ^{16}O (Refs. 36 and 37). We list separately cross sections calculated in the same (arbitrary) units and the ratio calculation/experiment normalized to the $4\text{-}8^+$ cross sections as indicated. The latter procedure would yield a unique DWBA normalization if the $4\text{-}8^+$ levels were pure $(h_{9/2})^2$. The $(h_{9/2}f_{7/2})$ mixtures are important, however, and therefore the DWBA normalization used in Table IV is model-dependent to a factor of about 2. We have in several instances used an average normalization based on the $4^+ + 6^+ + 8^+$ calculations for KH-II

TABLE IV. Comparison of experimental and calculated cross sections to the $(h_{9/2})^2$ multiplet in ^{210}Po.

	E_x [a] (MeV)	J^π	Wave function	^{210}Po [b]	$\int\sigma$ [c] (μb)	Calculated cross section [d] (arb.)	Calc./exp. [e]	EF [f]
(^{12}C, ^{10}Be)								
78 MeV	0	0^+	Pure	$h_{9/2}^2$	94 ± 15	0.146	0.28	3.57
			...		...	...	...	9.09 [g]
			MT			3.0	2.09	
			KH-II			3.58	3.30	
			KH-I			1.75	1.23 [g]	
			(t, α) [h]			1.30	0.92 [g]	
	1.19	2^+	Pure	$h_{9/2}^2$	36 ± 9	1.35	0.67	1.49
			...		...	...	...	3.79 [g]
			MT			1.52	2.77	
			KH-II			0.64	1.51	
	1.46	$4\text{-}8^+$	Pure	$h_{9/2}^2$	46 ± 11	0.26	1.0 [e]	
			MT			0.70	1.0 [e]	
			KH-II			0.54	1.0 [e]	
(^{16}O, ^{14}C)								
104 MeV	0	0^+	Pure	$h_{9/2}^2$	47 ± 15	0.10	0.53	1.89
			...		...	...	...	6.60 [g]
			MT			6.41	8.67	
			KH-II			7.60	14.50	
			KH-I			3.49	5.52 [g]	
			(t, α) [h]			2.45	3.86 [g]	
	1.14	2^+	Pure	$h_{9/2}^2$	23 ± 10	1.08	1.25	0.80
			...		...	...	...	2.80 [g]
			MT			3.34	9.36	
			KH-II			1.23	4.89	
	1.47	$4\text{-}8^+$	Pure	$h_{9/2}^2$	37 ± 14	0.14	1.0 [e]	
			MT			0.58	1.0 [e]	
			KH-II			0.41	1.0 [e]	

[a] From Table I ($\leq \pm 40$ keV).

[b] Wave functions used for ^{210}Po: MT (Ref. 35), KH-II (Ref. 34, approximation II), KH-I (Ref. 34, approximation I), (t, α) (Ref. 15). Cohen-Kurath wave functions used for ^{16}O and ^{12}C (Ref. 37, set a).

[c] From Table I ($\theta \sim 40\text{–}80°$ c.m.).

[d] DWBA calculation using V_{SI} form factor (see text).

[e] Ratio theory/experiment normalized to calculated sum of 4^+, 6^+, and 8^+ levels for wave functions noted, except for KH-I and (t, α) (see footnote g).

[f] Enhancement of cross section as deduced from ratio of experiment to theory using DWBA normalization to 4^+, 6^+, and 8^+ states assuming pure $(h_{9/2})^2$ or mixed wave functions for the latter (see footnote g).

[g] Using an average of the normalization for the 4^+, 6^+, and 8^+ states obtained with MT and KH-II wave functions.

[h] Using single-particle amplitudes deduced from an ^{210}Po(t, α) experiment (Ref. 15) and constructive phases.

and MT wave functions (denoted by superscript in Table IV). The results obtained with and without corrections for recoil are similar, except for the absolute normalization (see Appendix). The calculations presented in Table IV indicate the following: (1) as expected, the pure $(h_{9/2})^2$ wave functions grossly underestimate the 0^+ g.s. cross sections; (2) the KH-II and MT calculations both overestimate the 0^+ g.s. and 2^+ cross sections by factors 2 to 15; (3) the 0^+ g.s. calculations based on KH-I or the wave functions deduced from ^{210}Po(t, α) are in good agreement with the experimental data for (^{12}C, ^{10}Be) but overestimate the (^{16}O, ^{14}C) cross sections. The latter cross sections, however, are more sensitive to configuration mixing in the projectile.

2. Enhancement of 0^+ g.s. and 2^+ cross sections

Yoshida[38] and others[39] have shown that the short-range attractive nuclear forces which lower the energies of the first 0^+, 2^+, 3^-, $\cdots$ states in nuclei introduce correlations which also enhance two-nucleon transfers to these states. Such correlations, of course, are included in "realistic" shell-model calculations such as KH and MT. These correlations, e.g., introduce constructive phases for the terms comprising the coherent sum included in the form factor and can result in a large enhancement of the cross sections compared to other transitions.

In the last column of Table IV we list enhancement factors EF deduced for the ^{210}Po 0^+ g.s. and 2^+ states as follows: we define EF to be the enhancement in the observed cross section compared to that expected for a pure shell-model configuration, in this case $(h_{9/2})^2$. We give values of EF deduced with different DWBA normalizations: the 0^+ g.s. values $EF = 3.57$ and 1.89 for (^{12}C, ^{10}Be) and (^{16}O, ^{14}C), respectively, have been deduced assuming pure $(h_{9/2})^2$ wave functions for the 4-8^+ multiplet whereas $EF = 9.09$ and 6.60 have been deduced using an average normalization from KH-II and MT calculations. The latter EF values are presumably more realistic. Using the "realistic" normalizations we conclude that the ^{210}Po 0^+ g.s. cross section is enhanced (as defined above) by a factor ~8 and the 2^+ cross section by a factor ~3 in the heavy-ion two-proton-transfer reactions (^{12}C, ^{10}Be) and (^{16}O, ^{14}C).

We may compare the value $EF \sim 8$ for ^{210}Po g.s. ($Z = 84$, $N = 128$) with the enhancement factors deduced by von Oertzen[40] for (^{16}O, ^{14}C) on several nuclei $Z \sim 26$ to 64 ($N \sim 26$ to 82). Using the semi-

TABLE V. Comparison of exact and no-recoil DWBA calculations.

Reaction	Q (MeV)	E_x (MeV)	L	Exact DWBA [a] θ_{peak} [d] (deg.)	Exact DWBA [a] $\sigma_L^{DW}(\theta)$ [e] (μb/sr)	No-recoil DWBA [b] θ_{peak} [d] (deg.)	No-recoil DWBA [b] $\sigma_L^{DW}(\theta)$ [e] (μb/sr)	Ratio [c] exact / no recoil
^{208}Pb(^{12}C, ^{10}Be)	−18.6	0	0	63	35.2	63	5.2	6.8
$E_L = 78$ MeV			2	62	141.5	63	21.1	6.7
			6	62	80.6	63	12.1	6.7
	−24.6	6	0	89	5.9	82	0.40	14.8
			2	80	29.6	80	1.91	15.5
			6	73	43.4	73	2.63	16.5
^{208}Pb(^{16}O, ^{14}C)	−13.6	0	0	62	47.4	62	21.1	2.24
$E_L = 104$ MeV			2	62	170.5	62	76.3	2.23
			6	62	61.8	63	27.9	2.21
	−18.6	5	0	65	40.0	67	7.6	5.25
			2	65	166.5	67	31.5	5.28
			6	65	105.8	65	19.9	5.32
	−24.6	11	0	78	5.21	80	0.42	12.4
			2	77	28.1	78	2.16	13.0
			6	72	48.9	73	3.51	13.9

[a] Exact finite-range DWBA calculation (Ref. 53) assuming a diproton transfer with $\tilde{n}_2\tilde{l}_2 = 1S$ and $\Lambda_2 = L$ (see text). Optical parameters (Woods-Saxon): $V = -40$ MeV, $W = -15$ MeV, $R = 1.31 \times (A_1^{1/3} + A_2^{1/3})$ fm and $a = 0.45$ fm.

[b] Same as exact DWBA calculation (a) above except no-recoil approximation is made (Refs. 20, 49, and 52).

[c] Ratio of peak cross sections for exact and no-recoil DWBA calculations [see footnotes (a) and (b)].

[d] Calculated position (c.m.) of maximum in the differential cross section.

[e] The maximum value of the DWBA differential cross section (i.e., $\theta = \theta_{peak}$). These values do not include the spectroscopic amplitudes for the projectile or target (see text).

classical transfer probabilities, he obtains[40] [relative to ^{54}Fe(^{16}O, ^{14}C)^{56}Ni g.s.[41]] $EF \sim 5$ for ^{88}Sr(^{16}O, ^{14}C)^{90}Zr g.s.[41] and $EF \sim 20$ for ^{144}Sm-(^{16}O, ^{14}C)^{146}Gd g.s.[40] The enhancement factors obtained for the two-proton transfer (^{16}O, ^{14}C) in the region $Z \sim 26$ to 84 are found to be comparable (when defined in an analogous manner) with those deduced[39] from two-neutron transfers (t, p) and (p, t) within the corresponding neutron shells (i.e., $N \sim 26$ to 84). This implies that the p-p and n-n correlations are comparable within the same shell.

The enhancement ($EF \sim 3$) of the 2^+ quadrupole state at 1.18 MeV is comparable to the $B(E2)$ enhancement observed in inelastic scattering from this state[14] [$G_\lambda = 3.5 \pm 1.5$ single-particle units (s.p.u.), see Table III]. The 3^- octupole state at 2.387 MeV was not observed in the present experiment. Although this state is very collective[14] ($G_\lambda = 46 \pm 15$ s.p.u.) the main two-proton configurations in this state would be $(h_{9/2} i_{13/2})_{3^-}$ and $(f_{7/2} i_{13/2})_{3^-}$. The former dominant configuration is not favored ($0^+ \rightarrow j_< j'_>, J \neq j + j'$) while the latter configuration is expected[34, 35] to have a small amplitude (<0.1). Thus, we would not expect this level to be strongly excited in (^{12}C, ^{10}Be) or (^{16}O, ^{14}C) compared to other levels in the energy region $E_x \sim 2$–3 MeV.

VII. DISCUSSION: LEVELS IN ^{210}Po OBSERVED WITH (^{12}C, ^{10}Be) AND (^{16}O, ^{14}C)

In the following sections we discuss the levels observed in this experiment and suggest their predominant configurations. These suggested "assignments" are based on a comparison with known[11–17] levels in ^{210}Po and energies and cross sections calculated with shell-model wave functions[34–37] (e.g., Figs. 9–11) and are therefore very model-dependent. The experimental excitation energies are those listed in Table III, unless otherwise noted.

In a preliminary report of this experiment,[42] initial calculations indicated that the $(f_{7/2})^2$ and $(f_{7/2} f_{5/2})$ configurations would be dominant. The present calculations, however, using "realistic" wave functions and fewer approximations give different results particularly for levels $E_x \sim 4$ MeV.

All levels in ^{210}Po $E_x < 4.98$ MeV are particle stable. The proton, neutron, and α separation energies are 4.98, 7.65, and 5.41 MeV, respectively, while the two-proton and two-neutron separation energies are 8.78 and 14.62 MeV, respectively.

A. Levels $E_x < 6.0$ MeV

Below $E_x = 6.0$ MeV, levels seen in both (^{12}C, ^{10}Be) and (^{16}O, ^{14}C) must be due to excitation of ^{210}Po, since the first known excited state in ^{14}C is at $E_x = 6.09$ MeV (see Sec. III A). Levels seen only in (^{12}C, ^{10}Be) $E_x > 3.3$ MeV could be due to excitation of either ^{210}Po or ^{10}Be, but as discussed in Sec. III A most groups $E_x < 6$ MeV are believed to be levels in ^{210}Po.

1. $E_x = 0$, 1.19, and 1.46 MeV

These levels are well separated from all other expected levels and are therefore assumed to be the 0^+, 2^+, and unresolved $4^+ + 6^+ + 8^+$ (mainly 4^+) levels seen in other work (see Table III).

2. $E_x = 2.27$ MeV

This group appears to consist of more than one level (see Fig. 4 and Table I). Calculations (Figs. 9–11) suggest that $(f_{7/2})^2$ 0^+ is the main component although $(f_{7/2} h_{9/2})$ 6^+ and 8^+, known to be at 2.188 and 2.336 MeV, respectively, should also be excited particularly in (^{12}C, ^{10}Be). The $(f_{7/2})^2$ 0^+ level is calculated by Ma-True[35] to be at $E_x = 2.19$ MeV (2.68 MeV, KH-II[34]).

3. $E_x = 2.56$ MeV

Calculations indicate that this state is probably the $(h_{9/2} f_{7/2})$ 2^+ level [mixed with $(f_{7/2})^2$ 2^+] predicted to be at 2.451 MeV by Ma-True[35] (2.43 MeV, KH-II).[34] This is not consistent with (α, t) and (^{3}He, d) work, however, which has all $(h_{9/2} f_{7/2})$ strength below 2.43 MeV.[16, 17]

4. $E_x = 2.85$ and 3.05 MeV

These levels are close in energy to known $(h_{9/2} i_{13/2})$ levels (11^- and $5\text{-}9^-$, respectively). Our calculations, however, predict significant strength only to the 9^- state (Figs. 9–11). Most of the strength should go to the $(f_{7/2})^2$ 2^+ and $(f_{7/2})^2$ 4^+ and 6^+ levels. The former is calculated by Ma-True to be at 2.65 MeV (2.97 MeV, KH-II) while the latter are at 3.10 and 3.28 MeV (3.24 and 3.31 MeV, KH-II). Also, the relative cross sections seen in (^{12}C, ^{10}Be) and (^{16}O, ^{14}C) indicate small L transfers. This is consistent with these states being 2^+ and 4^+ ($+6^+$) rather than 11^- and 9^-.

5. $E_x = 3.41$ MeV

A group is seen in (^{12}C, ^{10}Be) at this energy but is absent (or very weak) in (^{16}O, ^{14}C). This group is consistent with a transition to ^{210}Po (g.s.) and ^{10}Be* (2^+), the latter being at 3.37 MeV. The width of this group, however, appears to be narrow compared to that expected from broadening[3] due to γ decay in flight (300–400 keV). An alternate possibility is that this level is the $(f_{7/2})^2$ 6^+ state in ^{210}Po, but this is not very consistent with the calculations, particularly the expected 4^+-6^+

splitting (see Figs. 9–11). There is a level seen in ^{210}Po(p, p') with weak intensity at 3.437 MeV. This latter data would be most consistent with this being the $(f_{7/2}i_{13/2})$ 3^- state; however, calculations place this state at 3.70 MeV.

6. E_x=3.70 and 4.07 MeV

The calculations favor these states being mainly the $(f_{7/2}i_{13/2})$ 3^- and 5^- levels predicted by Ma-True[35] to be at 3.69 and 3.94 MeV, respectively (3.62 and 3.93 MeV, KH-II).[34] The level at 3.70 MeV, however, is populated more strongly in (^{12}C, ^{10}Be) than expected for the 3^- level and would be more consistent with a higher spin value [e.g., $(f_{7/2})^2$ 6^+]. Although there have been several negative-parity and/or collective states seen in this region (Table III) all are unassigned or assigned $J \geq 4$.

7. E_x=4.36 and 4.53 MeV

These groups appear to be most consistent with their being composed of members of the $(h_{9/2}p_{3/2})$ multiplet seen[16,17] in (α, t) and (^{3}He, d). The 4.53-MeV group is likely to be the $(h_{9/2}p_{3/2})$ 6^+ level predicted by Ma-True[35] to be at this energy (4.52 MeV, KH-II).[34]

There are several isomeric states in this region seen[12,13] in $(\alpha, 2n\gamma)$. These states, however, involve core excitation which is not believed to be an important mechanism in the (^{12}C, ^{10}Be) and (^{16}O, ^{14}C) reactions (see Sec. IV).

8. E_x=4.95 and 5.07 MeV

The 4.95- and 5.07-MeV levels [unresolved in (^{16}O, ^{14}C)] are calculated to be mainly $(f_{7/2}p_{3/2})$ 2^+ and 4^+ predicted by Ma-True[35] to be at 5.13 and 5.33 MeV (5.22 and 5.50 MeV, KH-II).[34] Excitation of the 16^+ isomeric state at 5.058 MeV[12,13] would not be likely since core excitation would be required. Also, L=16 is not particularly favored kinematically (see Appendix).

9. E_x=5.33, 5.53, and 5.81 MeV

Groups are observed at these energies with both (^{12}C, ^{10}Be) and (^{16}O, ^{14}C) although it is not clear that the same groups are excited in these reactions (see Table I). The group seen in (^{12}C, ^{10}Be) at E_x=5.53 is much stronger than any groups observed in (^{16}O, ^{14}C) near this energy (see Figs. 9–11). Also, there are no states predicted to be populated as strongly as is observed. This suggests two possibilities: the group at 5.53 MeV is due to ^{10}Be* (3.37 MeV) and ^{210}Po* (2.27 MeV), or it is an excited state of ^{210}Po not included in the shell-model basis considered here,[34,35] e.g., a state from the next oscillator shell. If the latter be the case, its structure and spin must be such that it would be preferentially populated in (^{12}C, ^{10}Be), e.g. $(j_<)^2$ and large J, respectively.

B. E_x>6 MeV

Above 6 MeV excitation many groups appear in either or both the (^{12}C, ^{10}Be) and (^{16}O, ^{14}C) spectra (see Table I). Any "assignments," however, are limited by the fact that the groups observed may be due to projectile excitation. A broad structure seen in (^{16}O, ^{14}C) $E_x \sim 7$ MeV appears (Fig. 3) to be due to ^{14}C*. The angular distribution to a part of this structure (E_x=7.25 MeV) is different from others (see Fig. 6), although the measurements contain considerable uncertainties due to background subtraction.

A level $E_x \sim 6.06$ MeV appears in both (^{12}C, ^{10}Be) and (^{16}O, ^{14}C) and is probably a level in ^{210}Po. Furthermore, identifiable peaks are observed in several (^{16}O, ^{14}C) spectra at $E_x \sim 8.7$, 9.4, 10.0, 10.7, 11.7, and 12.3 MeV (see Table I). The relatively narrow widths of these peaks (see Fig. 3) suggest that they are levels in ^{210}Po, although above E_x=8.78 MeV the two-proton configurations in ^{210}Po are unbound.

VIII. CONCLUSIONS

We may summarize the results presented above as follows:

(i) The two-proton-transfer reactions ^{208}Pb-(^{12}C, ^{10}Be)^{210}Po and ^{208}Pb(^{16}O, ^{14}C)^{210}Po appear to populate, preferentially, certain levels in ^{210}Po $E_x < 8$ MeV.

(ii) The measured angular distributions show no reliable L or J signature, which precludes model-independent assignments.

(iii) The theoretical calculations, however, exhibit features which are sensitive to the structure and spin of the projectile and target states (j and J) and suggest that the levels observed are selected states predicted by shell-model calculations.

(iv) The cross sections to the 0^+ (g.s.) and 2^+ (1.18-MeV) levels in ^{210}Po are found to be enhanced by factors ~8 and ~3, respectively, compared to those expected for pure $(h_{9/2})^2$ configurations. Calculations using "realistic" projectile and target shell-model wave functions, however, overestimate the 0^+ (g.s.) and 2^+ cross sections by factors of 2 to 15.

(v) The gross features of the observed spectra, $E_x \lesssim 7$ MeV, are reproduced by the calculations, and in particular the differences in the (^{16}O, ^{14}C) and (^{12}C, ^{10}Be) spectra. Among the shell-model wave functions used, those of Ma-True and Kuo-Brown (type I) yielded results most consistent with the data.

ACKNOWLEDGMENTS

We thank the staff and crew of the 88-in. cyclotron for providing us with the necessary ^{16}O and ^{12}C beams, C. Ellsworth for preparing the targets, and Björn Nilsson, L. Jardine, and M. A. Nagarajan for discussion and advice. We also thank Professor William True for supplying shell-model wave functions and R. DeVries for providing a copy of the finite-range DWBA program LOLA.

APPENDIX

In the following sections we discuss the kinematic and nuclear-structure effects present in the (^{12}C, ^{10}Be) and (^{16}O, ^{14}C) reactions on ^{208}Pb. Although we specifically discuss these reactions, many of the features noted will apply to other two-proton or two-neutron transfers involving ^{12}C, ^{16}O, and other projectiles.

A. Localization in R and l space

As will become apparent shortly, it is useful to calculate the localization of the (^{16}O, ^{14}C) and (^{12}C, ^{10}Be) reactions in terms of R and l, the projectile-target core separation and relative angular momentum, respectively. If we consider the ^{208}Pb-(^{12}C, ^{10}Be)^{210}Po (g.s.) $L=0$ transition and calculate the square of the matrix elements $\beta_L^M(l)$ as defined by Kunz[19] vs l for $L=M=0$, we find that the most important contributions occur in a narrow region (FWHM $\sim 5\hbar$) of l space centered at $l \sim 37\hbar$. The latter is about $10\hbar$ smaller than the classical l value calculated from the grazing angle θ_{gr} assuming Coulomb trajectories [$=\bar{\eta}\cot\frac{1}{2}\theta$ where $\bar{\eta}=\frac{1}{2}(\eta_i+\eta_f)$]. This difference reflects the influence of the attractive nuclear potential. In Fig. 12 we show the square of the integrand of the radial integral vs R for $l=37\hbar$. The largest contribution comes from a region near $R=12.3$ fm. This is ~1.5 fm (10%) smaller than the classical apsidal distance D_{gr}^{cl} [$=(\bar{\eta}/\bar{k})(1+\csc\frac{1}{2}\theta_{gr}$] and again demonstrates the effect of the nuclear potential.

A comparison of the theoretical calculations indicates that transfer cross sections are determined primarily by a narrow region of the asymptotic part of the form factor. We find that to a good approximation ($\lesssim 20\%$) relative transfer cross sections can be estimated by

$$\frac{d\sigma}{d\Omega} \propto |F_L(R_m)|^2 \sigma_L^{DW}(\theta), \tag{A1}$$

where $F_L(R_m)$ is the form factor at some radius

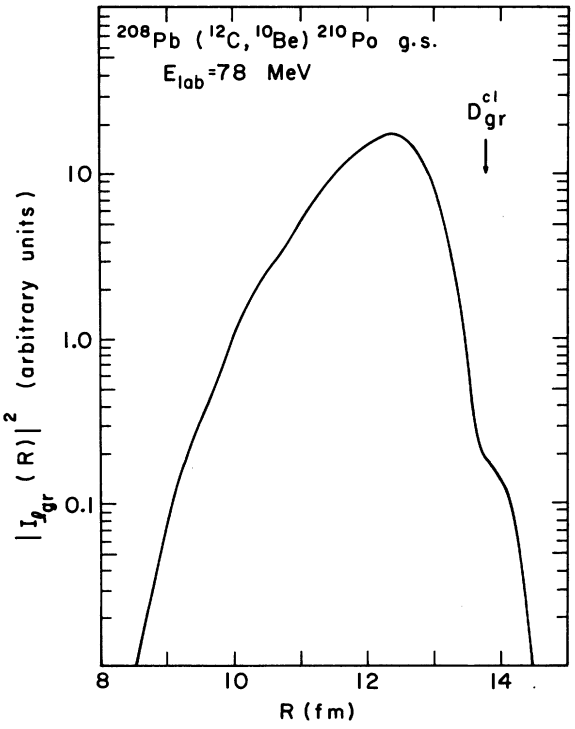

FIG. 12. The square of the integrand (averaged over 0.5 fm in R) for the radial integral determining β_L^M, $l=37\hbar$.

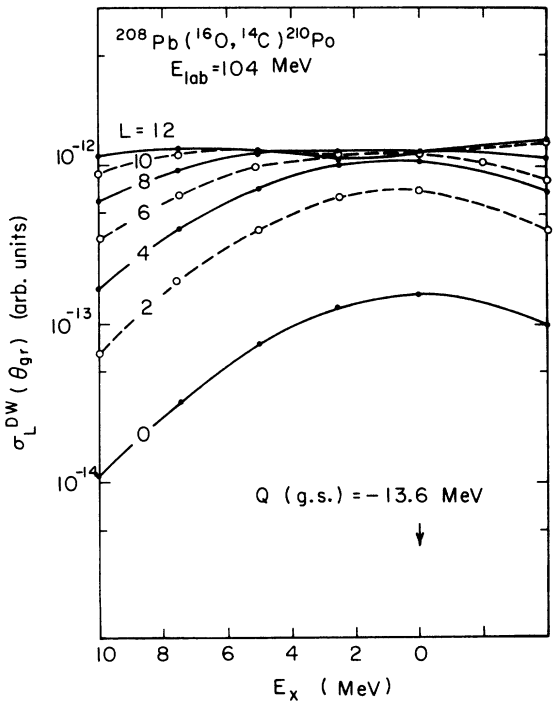

FIG. 13. The calculated dependence of no-recoil DWBA peak cross sections on L transfer and excitation energy for (^{16}O, ^{14}C) using a fixed form factor ($e^{-\kappa R}/\kappa R$, $\kappa=1.6$ fm^{-1}).

($R_m \cong 12$ fm) and $\sigma_L^{DW}(\theta)$ is the cross section for a fixed form factor. We have used Eq. (A1) extensively to calculate cross sections with $\sigma_L^{DW}(\theta)$ interpolated from DWBA calculations and $|F_L(R_m)|^2$ determined using either the CMI or SI methods.

B. Q windows

We can separate kinematic effects from nuclear structure by using an alternate form of Eq. (A1):

$$\frac{d\sigma}{d\Omega} \cong |f_L|^2 \sigma_L^{DW}(\theta), \tag{A2}$$

where f_L is a structure amplitude and $\sigma_L^{DW}(\theta)$ is the DWBA cross section calculated for a fixed form factor $h_0^{(1)*}(i\kappa R)(=e^{-\kappa R}/\kappa R)$. The quantity κ is obtained by fitting a Hankel function to the asymptotic part of the form factor. Note that our definition of σ_L^{DW} in Eq. (A2) includes the appropriate spin factors, e.g. $(2J_B+1)$, contained in the general expression Eq. (1).

We have performed calculations for (^{12}C, ^{10}Be) and (^{16}O, ^{14}C) vs Q and L. The DWBA program DWUCK[20] was used with a form factor $e^{-\kappa R}/\kappa R$, $\kappa = 1.6$ fm^{-1}. Optical-model parameters which fit the elastic scattering ^{16}O + ^{208}Pb ($E_L = 104$ MeV) and ^{12}C + ^{208}Pb ($E_L = 78$ MeV) were used[10]: $V = -40$ MeV, $W = -15$ MeV, $R = 1.31(A_1^{1/3} + A_2^{1/3})$ fm, and $a = 0.45$ fm. The DWBA angular distributions are bell shaped and peaked at an angle which changes with Q, but is nearly independent of L. The peak cross sections vs excitation in the residual nucleus E_x and L are shown in Fig. 13 for (^{16}O, ^{14}C). The calculated Q windows are essentially the same for (^{16}O, ^{14}C) and (^{12}C, ^{10}Be) but owing to the differences in g.s. Q values, the window centroid is at different E_x values in the two reactions. Inclusion of recoil shifts the Q windows ~ −4 MeV (see Sec. H of Appendix).

The general features are those expected from semiclassical theory[43-45]: a Gaussian window centered about some Q_{opt} with width $\propto L$. The calculated Q_{opt} values (~ − 14 MeV) are less negative than given by the sub-Coulomb formula of Buttle-Goldfarb[5] (Q_{opt} ~ − 25 MeV). Also, the Q windows appear to be much wider at higher bombarding energies, in agreement with semiclassical theory.[43-45] The quantity σ_L^{DW} (which includes $2J_B + 1 = 2L + 1$) increases rapidly with L only for $L \lesssim 6$. States with higher spin ($L > 6$) are therefore not particularly favored kinematically (see also Ref. 46).

C. CMI form factor

In this section we present details of the c.m. interaction (CMI) method of calculating the DWBA form factor for heavy-ion two-nucleon transfers, specifically (^{16}O, ^{14}C) and ^{12}C, ^{10}Be). The CMI method is an extension of the method used by Glendenning[22] to treat (p,t), (t,p), (^{3}He, n), etc. Since the interaction involves only the center-of-mass (c.m.) coordinates its matrix elements can be computed by transforming the coordinates of the two nucleons in the projectile and target into relative and c.m. motion with the aid of the Moshinsky-Talmi expansion.[47,48]

DWBA requires the evaluation of the six-dimensional integral[20,21]

$$T = \int d^3\vec{r}\, \chi_f^{(-)*}(\vec{k}_f, \vec{r}_f) \langle Bb|V|Aa\rangle \chi_i^{(+)}(\vec{k}_i, \vec{r}_i) \tag{A3}$$

for the reaction $A(a,b)B$. The coordinate system for two-nucleon transfer ($B = A+2$, $a = b+2$) is shown in Fig. 14. If the mass transfer is small compared with the masses (m_a, m_B) of a or B, then (A3) can be reduced to three dimensional integrals through use of the no-recoil approximations.[20,21] In some calculations, the use of the no-recoil approximation can introduce large errors.[18,19] We have investigated these effects and discuss them in Sec. H of the Appendix.

If the no-recoil approximations are used, the total form factor $\langle Bb|V|Aa\rangle$ can be written as

$$\langle Bb|V|Aa\rangle = \sum_{J_1 J_2 L} C_{J_1 J_2 L} F_{J_1 J_2 L}(R) Y_{LM}^*(\hat{\vec{R}}), \tag{A4}$$

where $C_{J_1 J_2 L}$ is a coupling coefficient and $\vec{R} = \vec{r}_{bA}$.

The radial form factor, $F_{J_1 J_2 L}(R)$, for two-nucleon transfer is obtained by expanding the motion of the transferred nucleon pair into relative and center-of-mass (c.m.) motion (see Fig. 14). The

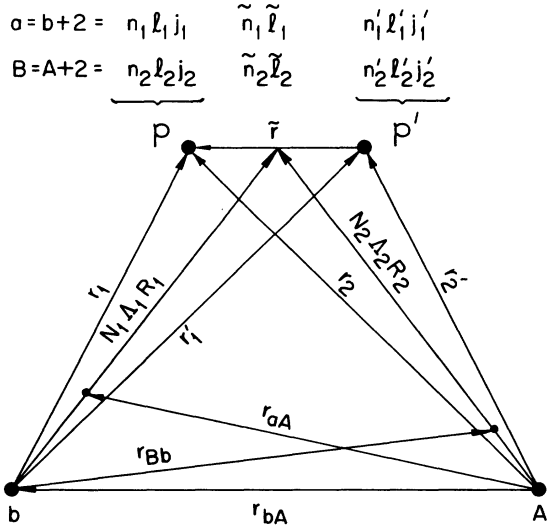

FIG. 14. Coordinate system used in the V_{CMI} method.

nucleon $p(p')$ is in the shell-model orbit $n_1 l_1 j_1$ $(n_1' l_1' j_1')$ in the nucleus "a" and in the state $n_2 l_2 j_2$ $(n_2' l_2' j_2')$ in "B." The c.m. radial wave functions of the dinucleon cluster relative to cores A and B are denoted by $U_{N_2\Lambda_2}(R_2)$ and $U_{N_1\Lambda_1}(R_1)$, respectively. The motion of p relative to p' in a and B is given by $u_{\tilde{n}_1\tilde{l}_1}(\tilde{r}/2)$ and $u_{\tilde{n}_2\tilde{l}_2}(\tilde{r}/2)$, respectively. The transferred nucleons are coupled to $J=J_1$ in nucleus a and $J=J_2$ in nucleus B. The total spins of A, B, a, and b are J_A, J_B, J_a, and J_b, respectively. The quantity L is the orbital angular momentum transfer between A and B. We consider the transfer of two identical nucleons and assume that the effective interaction is spin-independent and acts only on the c.m. of the transferred nucleon pair. The c.m. motion is approximated by Hankel functions and the Buttle-Goldfarb[5] method used to obtain the asymptotic part of the form factor as a function of R. One could also use the method of Sawaguri and Tobocman.[49] The interaction inducing the transition is that acting on the c.m. of the two nucleons in the projectile $a=b+2$ (post representation). Details are given in Ref. 23. The results are

$$F_L(R) \to \left(\sum \Omega_{12} G_1 G_2 N_{N_2\Lambda_2} A_{N_1\Lambda_1}\right) h_L^{(1)*}(i\kappa R) \quad \text{(A5a)}$$

$$\cong f_L h_0^{(1)*}(i\kappa R) , \quad \text{(A5b)}$$

where Ω_{12} is an overlap integral,[23] G_1 (G_2) are the projectile (target) structure factors,[22] and $N_{N_2\Lambda_2} \times A_{N_1\Lambda_1} h_L^{(1)*}(i\kappa R)$ is a projection of the asymptotic part of the c.m. motion of the transferred nucleons onto the projectile-target core separation R. The summation indicated in Eq. (A5a) is over all allowed states of relative and c.m. motion.

The form factor (A5a) is similar to that used in light-ion reactions,[22] except that the structure of the projectile appears explicitly. As pointed out previously,[23] the transfer process indicated by (A5a) involves structure factors for the stripping of two nucleons from the projectile and the simultaneous pickup of these by the target.

The quantum numbers $N_1, \Lambda_1, \tilde{n}_1, \tilde{l}_1$ etc. allowed in the sum (A5a) are constrained to satisfy the conditions[47,48]

$$2N_1 + \Lambda_1 + 2\tilde{n}_1 + \tilde{l}_1 = 2n_1 + l_1 + 2n_1' + l_1' \quad \text{(A6a)}$$

and

$$2N_2 + \Lambda_2 + 2\tilde{n}_2 + \tilde{l}_2 = 2n_2 + l_2 + 2n_2' + l_2'$$

with

$$\tilde{l}_1 = \tilde{l}_2 \quad \text{(A6b)}$$

and

$$|\Lambda_1 - \Lambda_2| \leq L \leq \Lambda_1 + \Lambda_2 .$$

We note, however, that (A6a) and (A6b) allow $\tilde{n}_2 \neq \tilde{n}_1$.

In the transfer of two identical nucleons from $1s_{1/2}$ orbitals [such as $(^3\mathrm{He}, n)$] only the relative $1S$ state of motion is available to the transferred nucleons. In contrast, for transfer of two identical nucleons from the $1p$ orbitals, relative motions in the $1S$, $2S$, and $1P$ states are allowed. Owing to antisymmetrization, the $1S$ and $2S$ states are spin singlet while the $1P$ state is spin triplet. A comparison of the terms in (A5a) indicates that for the ^{12}C and ^{16}O wave functions used here[36,37] (intermediate coupling) the target configurations with the largest $\tilde{n}\tilde{l} = 1S$ components are favored. Next in importance are $\tilde{n}\tilde{l} = 2S$ and finally $\tilde{n}\tilde{l} = 1P$. The latter terms are important if jj-coupled projectile wave functions are considered, since the jj to LS transformation included in (A5) introduces terms whose signs depend on whether $j_2(j_2') = l_2(l_2') + \frac{1}{2}$ or $l_2(l_2') - \frac{1}{2}$ i.e., $j_> j_>', j_< j_<'$ or $j_< j_>', j_> j_<'$ (see e.g. Ref. 23). There is also a J dependence within a multiplet $(j_2 j_2')_J$ which depends on the jj-to-LS transformation properties and the amount of relative $1S$ motion contained in the configuration $(j_2 j_2')_J$. These latter features are discussed in more detail in Secs. F and G of the Appendix.

The cross sections for the stripping reactions (^{16}O, ^{14}C g.s.) and (^{12}C, ^{10}Be g.s.) i.e., $J_a = J_b = 0$ on target nuclei $J_A = 0$ are given by

$$\frac{d\sigma}{d\Omega} = |f_L|^2 \sigma_L^{\mathrm{DW}}(\theta, \kappa) \quad \text{(A7)}$$

with $J_1 = 0$ and $L = J_2 = J_B$. The quantity $\sigma_L^{\mathrm{DW}}(\theta, \kappa)$ is the DWBA cross section (including $2L+1$) calculated with the form factor $h_0^{(1)*}(i\kappa R)$. Since the CMI form factor (A5) diverges at small radii it is necessary to introduce a cutoff in the DWBA radial integrals. The calculations for ^{208}Pb converge for $R_{co} \lesssim 9.5$ fm. This can be attributed to the strong absorption of the distorted waves for $R < 10$ fm, resulting in localization of the reaction in l and R space as discussed in Sec. A of the Appendix (Fig. 12).

Calculations[50] have been performed for ^{208}Pb-(^{12}C, ^{10}Be)^{210}Po and ^{208}Pb(^{16}O, ^{14}C)^{210}Po using the CMI method and approximation (A7). The clusters $U_{N\Lambda}(R)$ in the projectile and target are bound in Woods-Saxon wells ($R = 1.28A^{1/3}$ fm, $a = 0.76$ fm) at the appropriate two-proton separation energies, fitted with Hankel functions, and the sum indicated in (A5a) performed. Typical values of terms in (A5a) are given in Ref. 23. The coefficients $N_{N_1\Lambda_1}$, $N_{N_2\Lambda_2}$, and $A_{N_1\Lambda_1}$ are analogous to the coefficients $N_{n_1 l_1}, N_{n_2 l_2}$, and $A_{n_1 l_1}$ required for single-nucleon transfer[5] and exhibit the same properties, e.g., $N_{N_2\Lambda_2}$ increases rapidly with N_2 and less rapidly with Λ_2 while $A_{N_1\Lambda_1} \propto N_{N_1\Lambda_1}(\kappa_2)^{\Lambda_1}/(\kappa_1)^{(\Lambda_1+1)}$. Also

$\Omega_{12} \approx 0.9$ for $\tilde{n}_1 = \tilde{n}_2$ and decreases rapidly for $\tilde{n}_2 \neq \tilde{n}_1$.

D. Sum of interactions (SI)

A more basic formulation of the transfer process involves the matrix element of the interaction of each transferred nucleon with the projectile core (post representation). Thus if the interaction of the nucleons p and p' (see Fig. 14) in a $(=b+2)$ with the core b is denoted by the shell-model potentials $V_1(r_1)$ and $V_1'(r_1')$, then the transition amplitude involves the matrix element $\langle A, a | V_1(r_1) + V_1'(r_1') | B, b \rangle$. This matrix element is integrated over all internal coordinates and the result is a function of the separation R between the cores A and b, and of the transferred angular momentum L. Specific details of the SI method are given in the literature.[23,26,27]

Form factors for ^{208}Pb(^{12}C, ^{10}Be)^{210}Po (0^+) obtained with the SI method are shown in Fig. 15. The single-particle wave functions have been calculated at a single fixed binding energy in a Woods-Saxon well with $R = 1.20A^{1/3}$ fm, $a = 0.60$ fm, $V_{so} = 8$ MeV, and V adjusted. At large core separations, wave functions (nlj) with many nodes (large n) and yielding large relative $1S$ components (small l) are favored for a given L transfer. The effects of nuclear structure (projectile and target) are discussed in Secs. F and G of the Appendix.

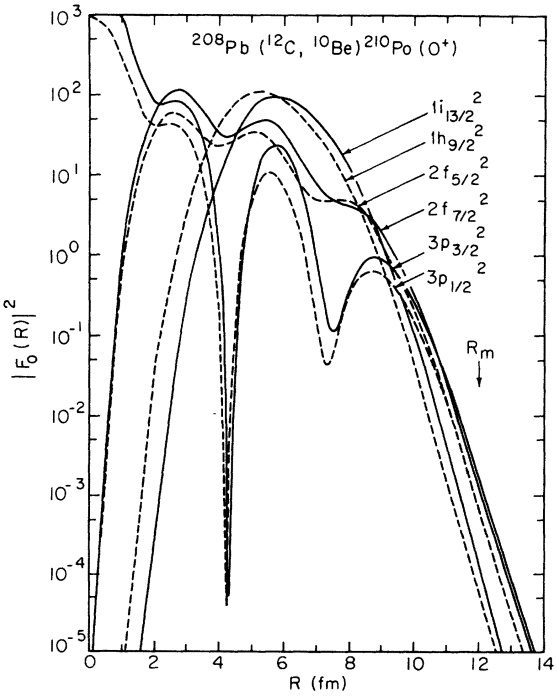

FIG. 15. The square of the form factor ($\mathrm{MeV}^2\,\mathrm{fm}^{-6}$) calculated ($V_{SI}$ method) for various $0^+ \rightarrow 0^+$ (^{12}C, ^{10}Be) transitions with Cohen-Kurath wave functions for ^{12}C (Refs. 36 and 37, set a) and pure configurations for ^{210}Po. R_m is the radius used in Eq. (A1) and is near the interaction radius deduced from the radial integrals (Fig. 12).

E. Comparison of SI and CMI methods

In Fig. 16 we compare (^{12}C, ^{10}Be) asymptotic form factors for the dominant configurations in ^{210}Po calculated with the CMI and SI methods. The CMI and SI calculations shown differ as follows: the CMI method treats the effective interaction V in (A3) as a spin-independent potential acting on a dinucleon cluster bound in the projectile at the two-nucleon separation energy while the SI method uses the sum interaction $V = V_1 + V_1'$ where V_1 and V_1' (which include a spin-orbit interaction) bind the individual nucleons in the projectile. Despite these intrinsic differences, the two calculations give qualitatively the same features.

There are, however, quantitative differences (factor $\gtrsim 2$ in $|F(R)|^2$) which are largest for unfavored transitions, i.e., those with poor relative S-state components. The $0^+ \rightarrow (1h_{9/2})^2$ and 0^+

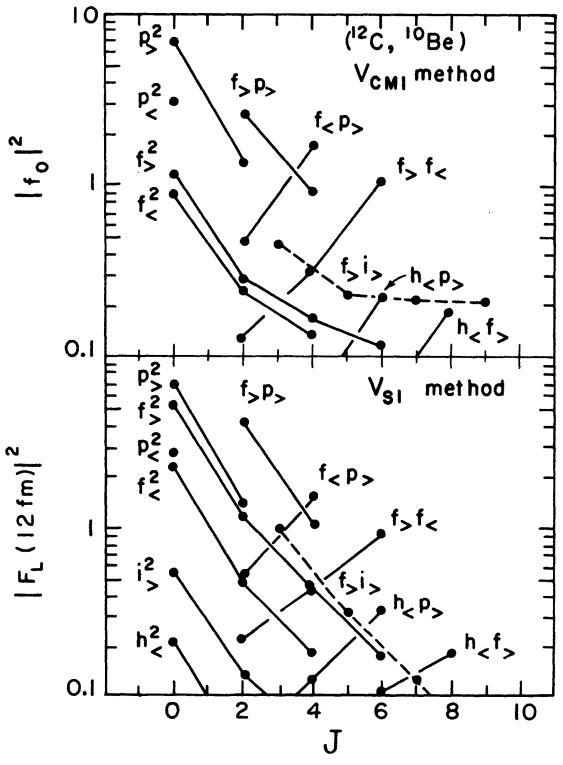

FIG. 16. Comparison of asymptotic form factors (arbitrary units) calculated for (^{12}C, ^{10}Be) (CK wave functions, Refs. 36 and 37) with (top) V_{CMI} method and (bottom) V_{SI} method. Levels in ^{210}Po of the form $[nlj \otimes n'l'j']_J$ are considered with j denoted by $j_<$ $(\equiv l - \frac{1}{2})$ and $j_>$ $(\equiv l + \frac{1}{2})$. Solid curves: positive parity; dashed curves: negative parity.

$\rightarrow (1i_{13/2})^2$ transitions, for example, are factors of 50 to 100 times weaker in the CMI calculations than in the SI method. Also, there appear to be differences in relative form factors for spin-orbit partners e.g., $p_{3/2}{}^2 - p_{1/2}{}^2$, $f_{7/2}{}^2 - f_{5/2}{}^2$, etc.

The systematics of the CMI calculations shown in Fig. 16 are very similar to those one would deduce for (^{3}He, n) from the appropriate structure factors.[51] In (^{3}He, n) or (p, t) one would have $|f_0|^2$ for 0^+ states $(3p_{3/2})^2 : (3p_{1/2})^2 : (2f_{7/2})^2 : (2f_{5/2})^2$ approximately the ratios 1 : 0.5 : 0.4 : 0.3 compared to 1 : 0.41 : 0.16 : 0.15 calculated for (^{12}C, ^{10}Be). The (^{3}He, n) and (^{12}C, ^{10}Be) cross sections, of course, depend on the behavior of $\sigma_L^{\mathrm{DW}}(\theta)$. If, however, Eq. (A7) would also apply to (^{3}He, n), i.e., if this reaction were localized in R space similar to (^{12}C, ^{10}Be) when one would expect 0^+ cross sections in proportion to the $|f_0|^2$ values noted above (provided the levels were nearly degenerate, i.e., had the same Q value). The close similarity between (^{12}C, ^{10}Be) and (^{3}He, n) structure factors arises from the large 1S relative diproton component contained in the ^{12}C wave functions of Cohen-Kurath.[36,37] (^{16}O, ^{14}C) would be expected to be more dissimilar since the ^{16}O wave functions are closer to jj coupling.

Detailed investigations of the CMI and SI methods as applied to two-neutron transfers, mainly (^{18}O, ^{16}O), may be found in the Refs. 23 and 25–27.

F. Projectile dependence (j dependence)

It is a distinguishing feature of heavy-ion reactions that the nucleons transferred to and from the projectile can be in single-particle states other than $1s_{1/2}$. This feature can result in a j selectivity such as that observed[10] in the (^{12}C, ^{11}B) and (^{16}O, ^{15}N) reactions. In (^{12}C, ^{11}B) the proton is transferred from a $1p_{3/2}$ orbit, i.e., a $j_>$ state ($\equiv l + \frac{1}{2}$) whereas in (^{16}O, ^{15}N) the orbit is $1p_{1/2}$, a $j_<$ orbit. This results in constraints on the allowed L transfer which together with the Q and L dependence of the cross sections leads to marked differences in the spectra observed for these reactions. The following features are observed[10]: (^{16}O, ^{15}N) favors $j_>$ final states, i.e., a transition from a $j_<$ projectile state to a $j_>$ final state is preferred, whereas for (^{12}C, ^{11}B), a $j_>$ projectile, the $j_>$ and $j_<$ target states are populated with comparable intensities (see Fig. 7).

Similarly one might expect a j selectivity for two-nucleon transfers from ^{16}O and ^{12}C. In the two-nucleon transfers considered here, however, such effects must enter via the structure factors Eq. (A5a) rather than constraints on L since $J_a = J_b = 0$. We have considered projectile wave functions consisting of a 0^+ core plus two protons in the $1p_{3/2}$ and $1p_{1/2}$ shell, i.e., $\alpha\, 1p_{3/2}{}^2 + \beta\, 1p_{1/2}{}^2$ where $\alpha^2 + \beta^2 = 1$. The form factor for transitions to final states of the form $(nlj)^2\ 0^+$ have then been calculated (SI method) vs the $(p_{1/2})^2$ mixing amplitude β^2. The results are shown in Fig. 17. At the top of Fig. 17 we indicate mixing ratios contained in various shell-model wave functions for two protons in ^{16}O and ^{12}C. These are: (1) pure jj coupling ($\beta^2 = 0$ and 1), (2) pure LS coupling ($\beta^2 \cong 0.33$), and (3) Cohen-Kurath wave functions[36,37] (CK ^{12}C, and CK ^{16}O, $\beta \cong 0.24$ and 0.80, respectively). One observes the following preferred $0^+ \rightarrow 0^+$ transfers:

$(j_>{}^2)0^+$ projectile configuration

$\rightarrow (j_<{}^2)0^+$ target configuration (A8a)

and

$(j_<{}^2)0^+$ projectile configuration

$\rightarrow (j_>{}^2)0^+$ target configuration. (A8b)

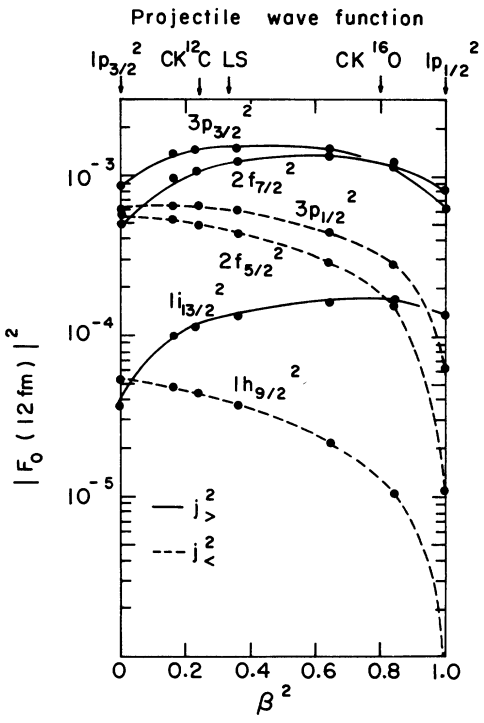

FIG. 17. Dependence of $|F_L(R_m)|^2$, $R_m = 12$ fm (see Sec. V) vs the projectile configuration: $\alpha p_{3/2}{}^2 + \beta p_{1/2}{}^2$ ($\alpha^2 + \beta^2 = 1$) for 0^+ levels in ^{210}Po of the form $(nlj)^2$. Solid curves: $j = j_> = l + \frac{1}{2}$, dashed curve: $j = j_< = l - \frac{1}{2}$. At the top mixing ratios for various projectile wave functions are indicated: pure $1p_{3/2}{}^2$; pure $1p_{1/2}{}^2$; pure $LS(^1S)$; and Cohen-Kurath ^{12}C and ^{16}O (Refs. 36 and 37, set a). V_{SI} method used.

Thus transitions involving pure jj-coupled wave functions (projectile and target) should exhibit a pronounced projectile dependence analogous to that observed for some single-nucleon transfers[10] (although the origin of the two effects are somewhat different).

Most of the j selectivity indicated by Eqs. (A8a) and (A8b) is destroyed by small amounts of configuration mixing in the projectile wave functions. Thus, e.g., a 20% admixture of $(p_{3/2})^2$ in ^{16}O increases the (^{16}O, ^{14}C) cross sections to $j_<^2$ final states ($3p_{1/2}{}^2$, $2f_{5/2}{}^2$, $1h_{9/2}{}^2$) by factors of 4 to 200. Even with "realistic" projectile wave functions,[36] however, measurable differences (~2) still exist between the calculated (^{12}C, ^{10}Be) and (^{16}O, ^{14}C) transition strengths.

G. Target-state dependence (J dependence)

The low-lying states of ^{210}Po populated in two-proton transfers on ^{208}Pb are expected to consist of levels formed by two protons in the shell-model orbits $nlj = 1h_{9/2}$, $2f_{7/2}$, $1i_{13/2}$, $2f_{5/2}$, $3p_{3/2}$, and $3p_{1/2}$. All states thus formed have positive parity except those involving the $1i_{13/2}$ "intruder" level from the next higher oscillator shell.

We have calculated the relative peak cross sections to these levels (SI method) with the aid of approximation (4). Cohen-Kurath wave functions (set a, Refs. 36 and 37) were used for the projectiles. The results are shown in Figs. 18 and 19 where we display calculated peak cross sections (no-recoil DWBA) for (^{12}C, ^{10}Be) and (^{16}O, ^{14}C) vs J, the spin of the final state in ^{210}Po. The final states $[nlj \otimes n'l'j']_J$ have been denoted by l and j, e.g., $f_> \equiv f_{7/2}$ (= a $j_>$ state); $f_< \equiv f_{5/2}$ (= a $j_<$ state), etc.

The calculated cross sections vs J increase or decrease with increasing J depending on the j values of the single-nucleon shell-model orbits. Two types of transitions are noted:

$$\text{Type I: } 0^+ \text{ (target)} \rightarrow [j_> \otimes j'_>]_J \text{ or } [j_< \otimes j'_<]_J \tag{A9a}$$

and

$$\text{Type II: } 0^+ \text{ (target)} \rightarrow [j_> \otimes j'_<]_J \text{ or } [j_< \otimes j'_>]_J \,. \tag{A9b}$$

Type I transitions are characterized by decreasing cross section with increasing J (within a multiplet) whereas Type II transitions exhibit the opposite behavior. The relative strength between different multiplets depends on the projectile, with a preference similar to that noted for the 0^+ states Eqs. (A8b). The J dependence of the type

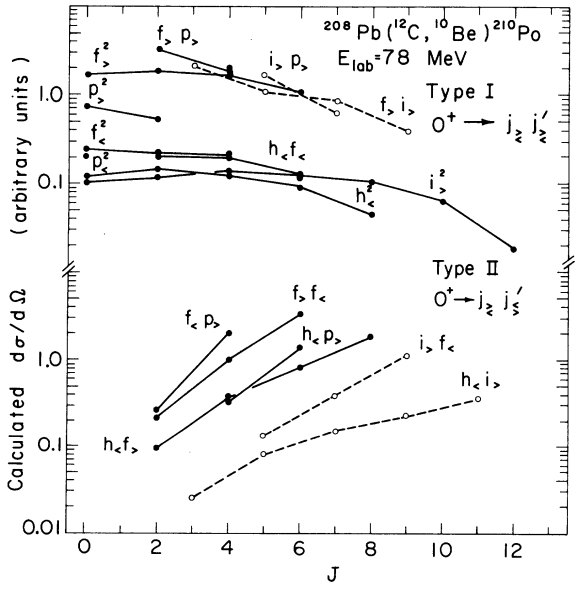

FIG. 18. The calculated peak cross sections (V_{SI} method, no-recoil DWBA) for ^{208}Pb(^{12}C, ^{10}Be) to levels in ^{210}Po of the form $[nlj \otimes n'l'j']_J$. The j values are denoted by $j_>$ ($\equiv l + \frac{1}{2}$) and $j_<$ ($\equiv l - \frac{1}{2}$). Solid curves: positive parity; dashed curves: negative parity. Cohen-Kurath wave functions used for ^{12}C (Refs. 36 and 37, set a).

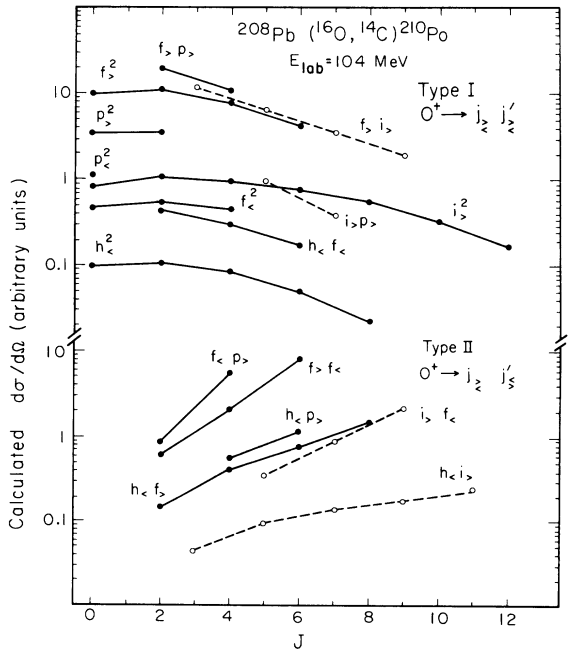

FIG. 19. The calculated peak cross sections (V_{SI} method, no-recoil DWBA) for ^{208}Pb(^{16}O, ^{14}C) to levels in ^{210}Po of the form $[nlj \otimes n'l'j']_J$. The j values are denoted by $j_>$ ($\equiv l + \frac{1}{2}$) and $j_<$ ($\equiv l - \frac{1}{2}$). Solid curves: positive parity; dashed curves: negative parity. Cohen-Kurath wave functions used for ^{16}O (Refs. 36 and 37, set a).

I and II transitions [Eqs. (A9a) and (A9b)] is directly related to the relative $1S$ singlet-spin motion in the ^{210}Po wave functions. In both types of transitions $1S$ relative motion is maximum for the coplanar orbits $J=j+j'$ or $j-j'$, but for type I singlet spin requires $J=j-j'$ and for type II, $J=j+j'$. This feature is not unique to heavy-ion reactions. In fact, the structure factors for (^{12}C, ^{10}Be) (CMI method) are very similar to those[51] for (^{3}He, n) since the CK wave functions for ^{12}C are predominantly LS coupled with a large relative $1S$ component. Thus, outside of differences due to kinematic effects, we would expect (^{12}C, ^{10}Be) and to some extent (^{16}O, ^{14}C) to populate the same states as in (^{3}He, n).

It should be noted that Eqs. (A8)–(A9) apply to transfer of identical nucleons from a p-shell projectile. Transfer of unlike nucleons i.e., as in (^{16}O, ^{14}N), can exhibit different characteristics.[41]

H. Recoil effects

One of the uncertainties associated with DWBA analyses of heavy-ion-induced transfer reactions concerns the effect of the recoil terms neglected in the usual DWBA calculations.[18,19,32] Recoil terms have been found to be important in single-nucleon transfers, where both the DWBA amplitudes and allowed L values are affected.[10,18,19,32]

We have estimated the effects of recoil for the two-proton transfer (^{16}O, ^{14}C) and (^{12}C, ^{10}Be) in the following manner: The two nucleons are assumed to be transferred as a cluster with relative motion $\tilde{n}_1\tilde{l}_1=\tilde{n}_2\tilde{l}_2=1S$ and singlet spin. Since $J_1=J_a=J_b=J_A=0$ only $L=J_2=J_B$ is allowed and from (A6), $\Lambda_1=0$ and $\Lambda_2=L$. The term with $\tilde{n}_1\tilde{l}_1=\tilde{n}_2\tilde{l}_2=1S$ and $L=\Lambda_2$ is usually the most important one in the sum (A5). The diproton clusters were bound in the projectile and target in Woods-Saxon potentials with $R=1.28A^{1/3}$ fm, $a=0.76$ fm, and V adjusted to fit the two-proton separation energies. No-recoil DWBA calculations were then performed with finite-range form factors generated using the Sawaguri-Tobocman method[49,52] and the DWBA amplitudes evaluated in a no-recoil DWBA program.[20] Calculations including recoil were next made using the same diproton wave functions but with a nonlocal form factor and DWBA amplitudes determined with an exact finite-range DWBA program.[53] The differences between the two sets of calculations represent the effect of recoil in the evaluation of the DWBA amplitudes.

Calculations have been performed for $L=0$, 2, and 6 for (^{16}O, ^{14}C), $Q=-13.6$, -18.6, and -24.6 MeV and (^{12}C, ^{10}Be), $Q=-18.6$ and -24.6 MeV. The results are presented in Table V. The following features are observed: (1) The relative cross sections for different L values (≤ 6) at the same Q value are not substantially altered by recoil. (2) The Q dependence of the cross sections, i.e., the Q windows (e.g., Fig. 13) are affected, however, with recoil introducing a shift in Q_{opt} of ~ -4 MeV. (3) The position of the maxima in the angular distributions calculated with and without recoil are similar and shift with Q value whereas the data do not (see Figs. 5–8). (4) The absolute DWBA normalization changes with the inclusion of recoil. Features similar to (2) and (4) have been noted by Buttle and Goldfarb[32] and DeVries and Kubo[19] in their analyses of single-nucleon transfers.

The recoil effects indicated in Table V can be simulated by application of empirically determined correction factors to the no-recoil DWBA cross sections, i.e.,

$$\sigma_L^{\text{DW}}(\text{recoil}) \cong \mathfrak{N}_1 \mathfrak{F}(Q) \sigma_L^{\text{DW}}(\text{no recoil}), \tag{A10a}$$

where

$$\mathfrak{F}(Q) = \exp(-0.162Q) \tag{A10b}$$

with

$$\begin{aligned} \mathfrak{N}_1 &= 0.25 \quad \text{for } (^{16}\text{O},\ ^{14}\text{C}) \\ &= 0.30 \quad \text{for } (^{12}\text{C},\ ^{10}\text{Be}). \end{aligned} \tag{A10c}$$

Equations (A10) were determined from calculations $L \leq 6$ and -24 MeV $\leq Q \leq -13$ MeV but may also be valid outside these limits. Alternate procedures to the one suggested above could also be derived from the recoil approximations given by Buttle and Goldfarb[32] or Nagarajan.[18]

The results noted above indicate that recoil corrections should be included in DWBA analyses of data spanning a range of several MeV in Q value. Thus, we have included the correction (A10a)–(A10c) in the calculation of the (^{12}C, ^{10}Be) and (^{16}O, ^{14}C) spectra (Figs. 10 and 11). The recoil correction reduces the calculated 0^+ g.s. cross sections by a factor ~ 2 compared with those to the strong state at $E_x \sim 5$ MeV. The enhancement factors (Table IV), however, do not depend sensitively on the recoil correction since all the calculations are for $Q \approx Q$ g.s.

I. Absolute cross sections

Since the (^{16}O, ^{14}C) and (^{12}C, ^{10}Be) DWBA calculations are sensitive to the form factor only in the asymptotic region (see Fig. 12), the absolute cross sections obtained are sensitive to bound-state parameters, etc., as well as the nuclear

wave functions. Using what are considered to be "realistic" bound-state parameters[10] and nuclear wave functions[35,36] we find that no-recoil DWBA underestimates the observed cross sections by factors of 1 to 6. Inclusion of recoil reduces the discrepancies such that $\sigma_{exp} \approx \frac{1}{2}$ to 3 times σ_{DWBA}. A more exact treatment of recoil is probably needed, however, before meaningful comparisons of absolute cross sections with DWBA can be made.

---

†Work performed under the auspices of the U.S. Atomic Energy Commission.

*Present address: Cyclotron Laboratory, Physics Department, University of Michigan, Ann Arbor, Michigan 48105.

‡Present address: Argonne National Laboratory, Argonne, Illinois.

§Permanent address: Hahn-Meitner Institute, Berlin, Germany.

‖On leave from Max Planck Institute, Hiedelberg, Germany.

[1]R. E. Hintz, F. B. Selph. W. S. Flood, B. G. Harvey, F. G. Resmini, and E. A. McClatchie, Nucl. Instrum. Methods 72, 61 (1969).

[2]B. G. Harvey, J. Mahoney, F. G. Pühlhofer, F. S. Goulding, D. A. Landis, J. C. Faivre, D. G. Kovar, M. S. Zisman, J. R. Meriwether, S. W. Cosper, and D. L. Hendrie, Nucl. Instrum. Methods 104, 21 (1972).

[3]M. S. Zisman, F. D. Becchetti, B. G. Harvey, D. G. Kovar, J. Mahoney, and J. Sherman, Phys. Rev. C 8, 1866 (1973).

[4]B. G. Harvey, H. Homeyer, J. Mahoney, and G. Gabor, LBL Progress Report, No. LBL-1666, 1972 (unpublished), p. 366.

[5]P. J. A. Buttle and L. J. B. Goldfarb, Nucl. Phys. 78, 409 (1966).

[6]J. Phys. (Paris) 32, Suppl. No. 11–12 (1971); R. J. Nickles *et al.*, Phys. Rev. Lett. 26, 1267 (1971); ORNL Report No. CONF-7200669, 1972 (unpublished); K. Nagatani, M. Ichimura, and A. Arima, Phys. Scr. 6, 289 (1972).

[7]T. Lauritsen and F. Ajzenberg-Selove, Nucl. Phys. 78, 1 (1966); D. E. Alburger *et al.*, Phys. Rev. 85, 1242 (1969).

[8]Taken from compilation of F. Ajzenberg-Selove, Nucl. Phys. A152, 1 (1970).

[9]M. Conjeaud, S. Harar, and C. Volant, in Proceedings of the European Physics Symposium, Aix-en-Provence, 1972 (unpublished), Vol. 2, p. II.40.

[10]D. G. Kovar, F. D. Becchetti, B. G. Harvey, F. G. Pühlhofer, J. Mahoney, D. W. Miller, and M. S. Zisman, Phys. Rev. Lett. 29, 1023 (1972); D. G. Kovar *et al.*, *ibid.* 30, 1075 (1973).

[11]L. J. Jardine and S. G. Prussin, Nucl. Phys. A190, 261 (1972).

[12]T. Yamazaki, Phys. Rev. C 1, 290 (1970); I. Bergström, B. Fant, and K. Wilström, Phys. Scr. 3, 103 (1971).

[13]B. Fant, Phys. Scr. 4, 175 (1971).

[14]C. Ellegaard, P. D. Barnes R. Eisenstein, E. Romberg, T. S. Bhatia, and T. R. Canada, Nucl. Phys. A206, 83 (1973).

[15]P. D. Barnes, E. Romberg, C. Ellegaard, R. F. Casten, Ole Hansen, T. J. Mulligan, R. Broglia, and R. Liotta, Nucl. Phys. A195, 146 (1972).

[16]R. Tickle and J. Bardwick, Phys. Lett. 36B, 32 (1971).

[17]W. A. Lanford, W. P. Alford, and H. W. Fulbright, private communication.

[18]M. A. Nagarajan, Nucl. Phys. A196, 34 (1972).

[19]R. M. DeVries and K. I. Kubo, Phys. Rev. Lett. 30, 325 (1973).

[20]P. D. Kunz, University of Colorado Reports Nos. COO-535-606 and COO-535-613 (unpublished).

[21]N. Austern, *Direct Nuclear Reactions Theories* (Wiley Interscience, New York, 1972), Chap. 5.

[22]N. K. Glendenning, Phys. Rev. 137, B102 (1965).

[23]R. Broglia, T. Kammuri, R. Liotta, A. Winther, and B. Nilsson, J. Phys. (Paris) 32, Suppl. No. 11–12, C6-151 (1971); R. Broglia, R. Liotta, A. Winther, B. Nilsson, and T. Kammuri (to be published); F. Becchetti *et al.*, LBL Report No. LBL-1972 (unpublished).

[24]R. Ascuitto and N. K. Glendenning, Nucl. Phys. A188, 185 (1972).

[25]A. J. Baltz and S. Kahana, Phys. Rev. Lett. 29, 1267 (1972).

[26]R. Ascuitto and N. K. Glendenning, unpublished.

[27]A. Roberts, Nucl. Phys. A196, 465 (1973).

[28]J. S. Larsen, J. L. C. Ford, Jr., R. M. Gaedke, K. S. Toth, J. B. Ball, and R. L. Hahn, Phys. Lett. 42B, 205 (1972).

[29]F. D. Becchetti, P. R. Christensen, V. I. Manko, and R. J. Nickles, Phys. Lett. 43B, 279 (1973).

[30]H. J. Körner, G. C. Morrison, L. R. Greenwood, and R. H. Seimssen, Phys. Rev. C 7, 107 (1973).

[31]J. V. Maher, K. A. Erb, and R. W. Miller, Phys. Rev. C 7, 651 (1973).

[32]P. J. A. Buttle and L. J. B. Goldfarb, Nucl. Phys. A176, 299 (1971).

[33]Y. E. Kim and J. O. Rasmussen, Nucl. Phys. 47, 184 (1963); 61, 173 (1965).

[34]G. H. Herling and T. T. S. Kuo, Nucl. Phys. A181, 113 (1972); Naval Research Laboratory Memorandum Report No. 2258, 1971 (unpublished).

[35]C. W. Ma and W. W. True, Phys. Rev. C 8, 2313 (1973); W. W. True, private communication.

[36]S. Cohen and D. Kurath, Nucl. Phys. A101, 1 (1967).

[37]S. Cohen and D. Kurath, Nucl. Phys. A141, 145 (1970).

[38]S. Yoshida, Nucl. Phys. 33, 685 (1962).

[39]N. K. Glendenning, Phys. Rev. 156, 1344 (1966); UCRL Report No. UCRL 18225 (unpublished).

[40]W. von Oertzen, H. G. Bohlen, and B. Gebauer, Nucl. Phys. A207, 91 (1973).

[41]P. R. Christensen, V. I. Manko, F. D. Becchetti, and R. J. Nickles, Nucl. Phys. A207, 33 (1973).

[42]F. D. Becchetti *et al.*, Bull. Am. Phys. Soc. 18, 714 (1973); LBL Progress Report No. LBL-1666, 1972 (unpublished), p. 95.

[43]D. Trautmann and K. Alder, Helv. Phys. Acta 43, 363 (1970); K. Alder and D. Trautmann, Nucl. Phys. A178, 60 (1971).

[44]A. Winther, J. Phys. (Paris) 32, Suppl. No. 11–12, C6-83 (1971); R. Broglia and A. Winther, Phys. Rep. 4C, 153 (1972).
[45]K. Alder, R. Morf, M. Pauli, and D. Trautmann, Nucl. Phys. A191, 399 (1972).
[46]D. Kovar, in Proceedings of the Argonne National Laboratory Heavy Ion Symposium, Argonne National Laboratory, 1973 (unpublished); LBL Report No. LBL-1654 (unpublished).
[47]I. Talmi, Helv. Phys. Acta 25, 185 (1952); M. Moshinsky, Nucl. Phys. 13, 104 (1959).
[48]T. A. Brody and M. Moshinsky, *Tables of Transformation Brackets* (Gordon and Breach, New York, 1967).
[49]T. Sawaguri and W. Tobocman, J. Math. Phys. 8, 2223 (1967).
[50]F. D. Becchetti, program HITN (unpublished) (Moshinsky-bracket routine written by M. S. Zisman); LBL Report No. LBL-1972 (unpublished).
[51]N. K. Glendenning, UCRL Report No. UCRL-18268, 1968 (unpublished).
[52]W. Tobocman, program RDRC (unpublished).
[53]R. DeVries, program LOLA (unpublished).